Shin RW, Iwaki T, Kitamoto T, Tateishi J. 1991. Hydrated autoclave pretreatment enhances tau immunoreactivity in formalin-fixed normal and Alzheimer's disease brain tissues. Lab Invest. 64:693–702.

Shin RW, Kruck TP, Murayama H, Kitamoto T. 2003. A novel trivalent cation chelator Feralex dissociates binding of aluminum and iron associated with hyperphosphorylated tau of Alzheimer's disease. Brain Res. 961:139–146.

Shin RW, Ogino K, Shimabuku A, Taki T, Nakashima H, Ishihara T, Kitamoto T. 2007. Amyloid precursor protein cytoplasmic domain with phospho-Thr668 accumulates in Alzheimer's disease and its transgenic models: a role to mediate interaction of Abeta and tau. Acta Neuropathol. 113:627–636.

Suurmeijer AJ, Boon ME. 1993. Notes on the application of microwaves for antigen retrieval in paraffin and plastic tissue sections. Eur J Morphol. 31:144–150.

Thal DR, Sassin I, Schultz C, Haass C, Braak E, Braak H. 1999. Fleecy amyloid deposits in the internal layers of the human entorhinal cortex are comprised of N-terminal truncated fragments of Abeta. J Neuropathol Exp Neurol. 58:210–216.

Uchihara T, Kondo H, Akiyama H, Ikeda K. 1995. White matter amyloid in Alzheimer's disease brain. Acta Neuropathol. 90:51–56.

Wisniewski HM, Bancher C, Barcikowska M, Wen GY, Currie J. 1989. Spectrum of morphological appearance of amyloid deposits in Alzheimer's disease. Acta Neuropathol. 78:337–347.

Yamamoto A, Shin RW, Hasegawa K, Naiki H, Sato H, Yoshimasu F, Kitamoto T. 2002. Iron (III) induces aggregation of hyperphosphorylated tau and its reduction to iron (II) reverses the aggregation: implications in the formation of neurofibrillary tangles of Alzheimer's disease. J Neurochem. 82:1137–1147.

REPORT

The TRK-Fused Gene Is Mutated in Hereditary Motor and Sensory Neuropathy with Proximal Dominant Involvement

Hiroyuki Ishiura,[1] Wataru Sako,[3] Mari Yoshida,[4] Toshitaka Kawarai,[3] Osamu Tanabe,[3,5] Jun Goto,[1] Yuji Takahashi,[1] Hidetoshi Date,[1] Jun Mitsui,[1] Budrul Ahsan,[1] Yaeko Ichikawa,[1] Atsushi Iwata,[1] Hiide Yoshino,[6] Yuishin Izumi,[3] Koji Fujita,[3] Kouji Maeda,[3] Satoshi Goto,[3] Hidetaka Koizumi,[3] Ryoma Morigaki,[3] Masako Ikemura,[7] Naoko Yamauchi,[7] Shigeo Murayama,[8] Garth A. Nicholson,[9] Hidefumi Ito,[10] Gen Sobue,[11] Masanori Nakagawa,[12] Ryuji Kaji,[3,*] and Shoji Tsuji[1,2,13,*]

Hereditary motor and sensory neuropathy with proximal dominant involvement (HMSN-P) is an autosomal-dominant neurodegenerative disorder characterized by widespread fasciculations, proximal-predominant muscle weakness, and atrophy followed by distal sensory involvement. To date, large families affected by HMSN-P have been reported from two different regions in Japan. Linkage and haplotype analyses of two previously reported families and two new families with the use of high-density SNP arrays further defined the minimum candidate region of 3.3 Mb in chromosomal region 3q12. Exome sequencing showed an identical c.854C>T (p.Pro285-Leu) mutation in the TRK-fused gene (*TFG*) in the four families. Detailed haplotype analysis suggested two independent origins of the mutation. Pathological studies of an autopsied patient revealed TFG- and ubiquitin-immunopositive cytoplasmic inclusions in the spinal and cortical motor neurons. Fragmentation of the Golgi apparatus, a frequent finding in amyotrophic lateral sclerosis, was also observed in the motor neurons with inclusion bodies. Moreover, TAR DNA-binding protein 43 kDa (TDP-43)-positive cytoplasmic inclusions were also demonstrated. In cultured cells expressing mutant TFG, cytoplasmic aggregation of TDP-43 was demonstrated. These findings indicate that formation of TFG-containing cytoplasmic inclusions and concomitant mislocalization of TDP-43 underlie motor neuron degeneration in HMSN-P. Pathological overlap of proteinopathies involving TFG and TDP-43 highlights a new pathway leading to motor neuron degeneration.

Hereditary motor and sensory neuropathy with proximal dominant involvement (HMSN-P [MIM 604484]) is an autosomal-dominant disease characterized by predominantly proximal muscle weakness and atrophy followed by distal sensory disturbances.[1] HMSN-P was first described in patients from the Okinawa Islands of Japan, where more than 100 people are estimated to be affected.[2] Two Brazilian HMSN-P-affected families of Okinawan ancestry have also been reported.[3,4]

The disease onset is usually in the 40s and is followed by a slowly progressive course. Painful muscle cramps and abundant fasciculations are observed, particularly in the early stage of the disease. In contrast to the clinical presentations of other hereditary motor and sensory neuropathies (HMSNs) presenting with predominantly distal motor weakness reflecting axonal-length dependence, the clinical presentation of HMSN-P is unique in that it involves proximal predominant weakness with widespread fasciculations resembling those of amyotrophic lateral sclerosis (ALS).[5] Distal sensory loss is accompanied later in the disease course, but the degree of the sensory involvement varies among patients. Neuropathological findings revealed severe neuronal loss and gliosis in the spinal anterior horns and mild neuronal loss and gliosis in the hypoglossal and facial nuclei of the brainstem, which indicates that the primary pathological feature of HMSN-P is a motor neuronopathy involving motor neurons, but not a motor neuropathy involving axons.[1,5] The posterior column, corticospinal tract, and spinocerebellar tract showed loss of myelinated fibers and gliosis. Neuronal loss and gliosis were found in Clarke's nucleus. Dorsal root ganglia showed mild to marked neuronal loss.[1,5] These observations suggest that HMSN-P shares neuropathological findings in part with those observed in familial ALS.[6]

Previous studies on Okinawan kindreds mapped the disease locus to chromosome 3q.[1] Subsequently, we identified two large families (families 1 and 2 in Figure 1A) affected by quite a similar phenotype in the Kansai area of Japan, located in the middle of the main island of Japan and far distant from the Okinawa Islands. We mapped the

[1]Department of Neurology, The University of Tokyo Graduate School of Medicine, 7-3-1 Hongo, Bunkyo-ku, Tokyo 113-8655, Japan; [2]Medical Genome Center, The University of Tokyo Hospital, 7-3-1 Hongo, Bunkyo-ku, Tokyo 113-8655, Japan; [3]Department of Clinical Neuroscience, The Tokushima University Graduate School of Medicine, 3-18-15 Kuramoto-cho, Tokushima 770-8503, Japan; [4]Department of Neuropathology, Institute for Medical Science of Aging, Aichi Medical University, 21 Karimata, Iwasaku, Nagakute-shi, Aichi 480-1195, Japan; [5]Department of Cell and Developmental Biology, University of Michigan Medical School, 109 Zina Pitcher Place, Ann Arbor, MI 48109-2200, USA; [6]Yoshino Neurology Clinic, 3-3-16 Konodai, Ichikawa, Chiba 272-0827, Japan; [7]Department of Pathology, Graduate School of Medicine, The University of Tokyo, 7-3-1 Hongo, Bunkyo-ku, Tokyo 113-8655, Japan; [8]Department of Neuropathology and the Brain Bank for Aging Research, Tokyo Metropolitan Institute of Gerontology, 35-2 Sakae-cho, Itabashi-ku, Tokyo 173-0015, Japan; [9]Molecular Medicine Laboratory and ANZAC Research Institute, University of Sydney, Sydney NSW 2139, Australia; [10]Department of Neurology, Kyoto University Graduate School of Medicine, 54 Kawahara-cho, Shogoin, Sakyo-ku, Kyoto 606-8507, Japan; [11]Department of Neurology, Nagoya University Graduate School of Medicine, 65 Tsurumai-cho, Showa-ku, Nagoya-shi, Aichi 466-0065, Japan; [12]Department of Neurology and Gerontology, Kyoto Prefectural University Graduate School of Medicine, 465, Kajii-cho, Kamigyo-ku, Kyoto 602-0841, Japan; [13]Division of Applied Genetics, National Institute of Genetics, Yata 1111, Mishima, Shizuoka 11-8540, Japan
*Correspondence: tsuji@m.u-tokyo.ac.jp (S.T.), rkaji@clin.med.tokushima-u.ac.jp (R.K.)
http://dx.doi.org/10.1016/j.ajhg.2012.07.014.

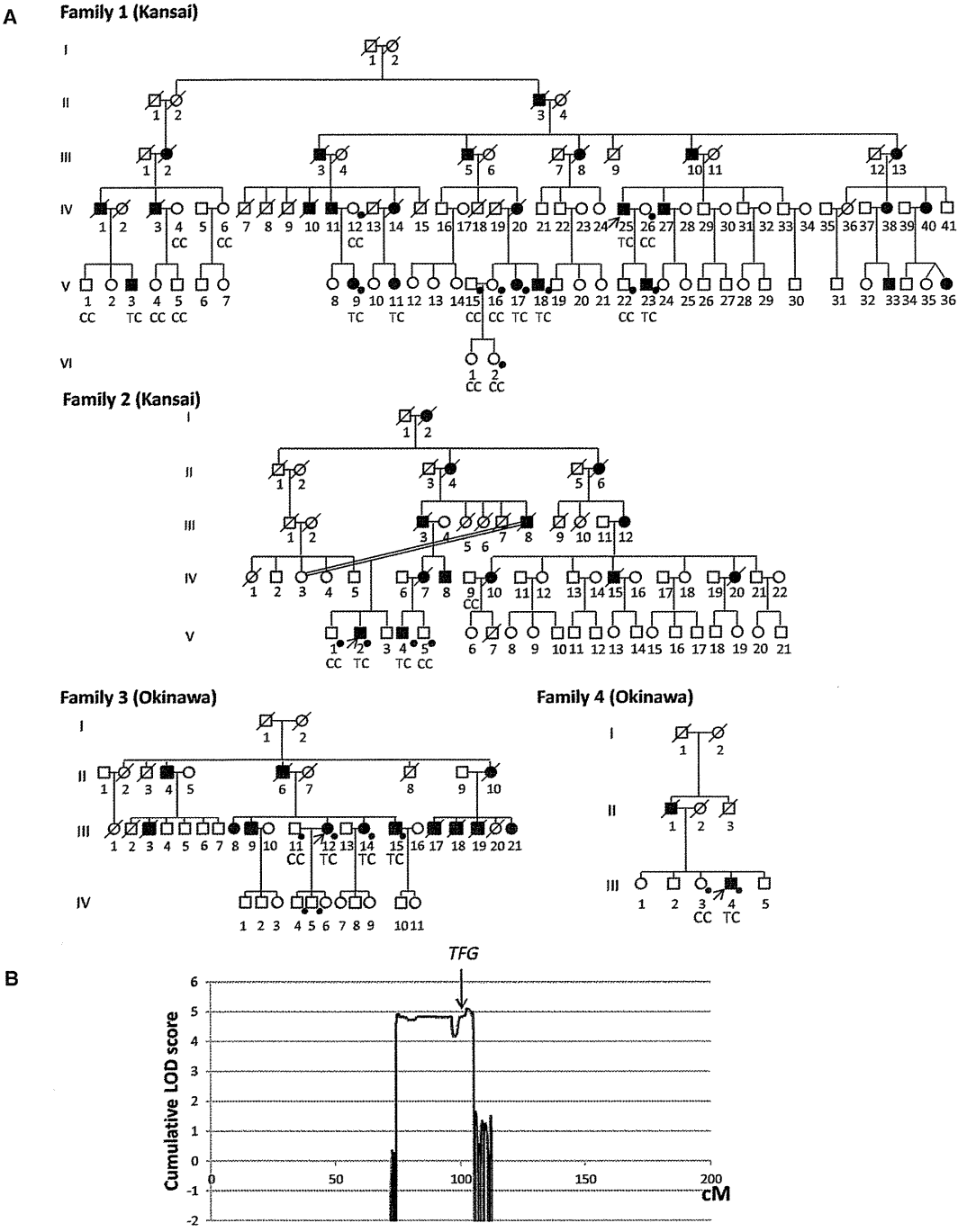

Figure 1. Pedigree Charts and Linkage Analysis
(A) Pedigree charts of families 1 and 2 (Kansai kindreds) and families 3 and 4 (Okinawan kindreds) are shown. Squares and circles indicate males and females, respectively. Affected persons are designated with filled symbols. A diagonal line through a symbol represents a deceased person. A person with an arrow is an index patient. Genotypes of *TFG* c.854 are shown in individuals in whom genomic DNA was analyzed. Individuals genotyped with SNP arrays for linkage analysis and haplotype reconstruction are indicated by dots. (B) Cumulative parametric multipoint LOD scores on chromosome 3 of all the families are shown.

disease locus to chromosome 3q,[7] overlapping with the previously defined locus, which strongly indicates that these diseases are indeed identical.

In addition to the large Kansai HMSN-P-affected families, we found two new Okinawan HMSN-P-affected families (families 3 and 4 in Figure 1A) in our study. In total, 9 affected and 15 unaffected individuals from the Kansai area and four affected and four unaffected individuals from the Okinawa Islands were enrolled in the study. Written informed consent was obtained from

Table 1. Clinical Characteristics of Patients with HMSN-P from Families 1 and 2 from Kansai and Families 3 and 4 from Okinawa

		Family 3			Family 4
	Families 1 and 2	**III-12**	**III-14**	**III-15**	**III-4**
Age at examination (years)	40s–50s	54	52	50	54
Age at onset (years)	37.5 ± 8	44	40	early 20s	41
Initial symptoms	shoulder dislocation and difficulty walking	proximal leg weakness	painful cramps	painful cramps and fasciculation	painful cramps and calf atrophy
Motor					
Proximal muscle weakness and atrophy	+	+	mild	+	+
Painful cramps	+	+	+	+	+
Fasciculations	+	+	+	+	+
Motor ability	bedridden after 10–20 years from disease onset	unable to walk; wheelchair	only mild difficulty climbing stairs	walk with effort	unable to walk; wheelchair
Bulbar symptoms	− ~ +	−	−	−	−
Sensory					
Dysesthesia	+	+	mild	+	+
Decreased tactile sensation	+	+	−	mild	+
Decreased vibratory sensation	+	mild	mild	mild	+
Reflexes					
Tendon reflexes	diminished	diminished	diminished	diminished	diminished
Pathological reflexes	−	−	−	−	−
Laboratory Tests and Electrophysiological Findings					
Serum creatine kinase level	270 ± 101 IU/l	761 IU/l	not measured	625 IU/l	399 IU/l
Hyperglycemia	4/13 patients	−	−	−	+
Hyperlipidemia	3/13 patients	+	−	+	+
Nerve conduction study	motor and sensory axonal degeneration	motor and sensory axonal degeneration	not examined	not examined	motor and sensory axonal degeneration
Needle electromyography	neurogenic changes with fibrillation potentials and positive sharp waves	neurogenic changes with fibrillation potentials and positive sharp waves	not examined	not examined	not examined

The clinical characteristics of the patients from families 1 and 2 were summarized in accordance with the previous studies.[5,6]

all participants. This study was approved by the institutional review boards at the University of Tokyo and the Tokushima University Hospital. Genomic DNA was extracted from peripheral-blood leukocytes or an autopsied brain according to standard procedures.

The clinical presentations of the patients from the four families are summarized in Table 1 and Table S1, available online. Characteristic painful cramps and fasciculations were noted at the initial stage of the disease in all the patients from the four families. Whereas some of the patients showed painful cramps in their 20s, the ages of onset of motor weakness (41.6 ± 2.9 years old) were quite uniform. These patients presented slowly progressive, predominantly proximal weakness and atrophy with diminished tendon reflexes in the lower extremities. Sensory impairment was generally mild. Indeed, one patient (III-4 in family 4) has been diagnosed with very slowly progressive ALS. Although frontotemporal dementia (FTD) is an occasionally observed clinical presentation in patients with ALS, dementia was not observed in these patients. Laboratory tests showed mildly elevated serum creatine kinase levels. Electrophysiological studies showed similar results in all the patients investigated and revealed a decreased number of motor units with abundant positive sharp waves, fibrillation, and fasciculation potentials. Sensory-nerve action potentials of the sural nerve were lost in the later stage of the disease. All these clinical findings were similar to those described in previous reports.[1,3,4]

To further narrow the candidate region, we conducted detailed genotyping by employing the Genome-Wide Human SNP array 6.0 (Affymetrix). Multipoint parametric linkage analysis and haplotype reconstruction were performed with the pipeline software SNP-HiTLink[8] and Allegro v.2[9] (Figure 1A). In addition to the SNP genotyping, we also used newly discovered polymorphic dinucleotide repeats for haplotype comparison (microsatellite marker 1 [MS1], chr3: 101,901,207–101,901,249; and MS2, chr3: 102,157,749–102,157,795 in hg18) around *TFG* (see Table S2 for primer sequences). The genome-wide linkage study revealed only one chromosome 3 region showing a cumulative LOD score exceeding 3.0 (Figure 1B), confirming the result of our previous study.[7] An obligate recombination event was observed between rs4894942 and rs1104964, thus further refining the telomeric boundary of the candidate region in Kansai families (Figure 2A). The Okinawan families (families 3 and 4) shared an extended disease haplotype spanning 3.3 Mb, consistent with a founder effect reported in the Okinawan HMSN-P-affected families,[1] thus defining the 3.3 Mb region as the minimum candidate region.

We then performed exon capture (Sequence Capture Human Exome 2.1 M Array [NimbleGen]) of the index patient from family 3 and subsequent passively parallel sequencing by using two lanes of GAIIx (100 bp single end [Illumina]) and a one-fifth slide of SOLiD 4 (50 bp single end [Life Technologies]). GAIIx and SOLiD4 yielded 2.60 and 2.76 Gb of uniquely mapped reads,[10] respectively. The average coverages were 29.0× and 26.8× in GAIIx and SOLiD4, respectively (Table S3 and Figure S1). In summary, 175,236 single nucleotide variants (SNVs) and 25,987 small insertions/deletions were called.[11] The numbers of exonic and splice-site variants were 14,189 and 127, respectively. In the minimum candidate region of 3.3 Mb, only 11 exonic SNVs were found, and only one was novel (i.e., not found in dbSNP) and nonsynonymous. Direct nucleotide-sequence analysis confirmed the presence of heterozygous SNV c.854C>T (p.Pro285Leu) in TRK-fused gene (*TFG* [NM_006070.5]) in all the patients from families 3 and 4 (Figure 3A and Figure S2[12]). Intriguingly, direct nucleotide-sequence analysis of all *TFG* exons (see Table S4 for primer sequences) of one patient from each of families 1 and 2 from the Kansai area revealed an identical c.854C>T (p.Pro285Leu) *TFG* mutation cosegregating with the disease (Figure 1A and Figure 3A). The base substitution was not observed in 482 Japanese controls (964 chromosomes), dbSNP, the 1000 Genomes Project Database, or the Exome Sequencing Project Database. Pro285 is located in the P/Q-rich domain in the C-terminal region of TFG (Figure 3B) and is evolutionally conserved (Figure 3C). PolyPhen predicts it to be "probably damaging." Because some of the exonic sequences were not sufficiently covered by exome sequencing (i.e., their read depths were no more than 10×) (Figure S1), direct nucleotide-sequence analysis was further conducted for these exonic sequences (Table S5). However, it did not reveal any other novel nonsynonymous variants, confirming that c.854C>T (p.Pro285Leu) is the only mutation exclusively present in the candidate region of 3.3 Mb. All together, we concluded that it was the disease-causing mutation.

Because we found an identical mutation in both Kansai (families 1 and 2) and Okinawan (families 3 and 4) families, we then compared the haplotypes with the c.854C>T (p.Pro285Leu) mutation in the Kansai and Okinawan families in detail. To obtain high-resolution haplotypes, we included custom-made markers, including MS1 and MS2, and new SNVs identified by our exome analysis, in addition to the high-density SNPs used in the linkage analysis. The two Kansai families shared as long as 24.0 Mb of haplotype, and the two Okinawan families shared 3.3 Mb, strongly supporting a common ancestry in each region. When the haplotypes of the Kansai and Okinawan families were compared, it turned out that these families do not share the same haplotype because the markers nearest to *TFG* are discordant at markers 48.5 kb centromeric and 677 bp telomeric to the mutation within a haploblock (Figure 2B). Although the possibility of rare recombination events just distal to the mutation cannot be completely excluded, as suggested by the population-based recombination map (Figure 2B), these findings strongly support the interpretation that the mutations have independent origins and provide further evidence that *TFG* contains the causative mutation for this disease.

Mutational analyses of *TFG* were further conducted in patients with other diseases affecting lower motor neurons (including familial ALS [n = 18], axonal HMSN [n = 26], and hereditary motor neuropathy [n = 3]) and revealed no mutations in *TFG*, indicating that c.854C>T (p.Pro285-Leu) in *TFG* is highly specific to HMSN-P.

In this study, we identified in all four families a single variant that appears to have developed on two different haplotypes. The mutation disrupts the PXXP motif, also known as the Src homology 3 (SH3) domain, which might affect protein-protein interactions. In addition, substitution of leucine for proline is expected to markedly alter the protein's secondary structure, which might substantially compromise the physiological functions of TFG.

By employing the primers shown in Table S6, we obtained full-length cDNAs by PCR amplification of the cDNAs prepared from a cDNA library of the human fetal brain (Clontech). During this process, four species of cDNA were identified (Figure S3A). To determine the relative abundance of these cDNA species, we used the primers shown in Table S7 to conduct fragment analysis of the RT-PCR products obtained from RNAs extracted from various tissues; these primers were designed to discriminate four cDNA species on the basis of the size of the PCR products. The analysis revealed that TFG is ubiquitously expressed, including in the spinal cord and dorsal root ganglia, which are the affected sites of HMSN-P (Figure S3B).

Neuropathological studies were performed in a *TFG*-mutation-positive patient (IV-25 in family 1) who died of

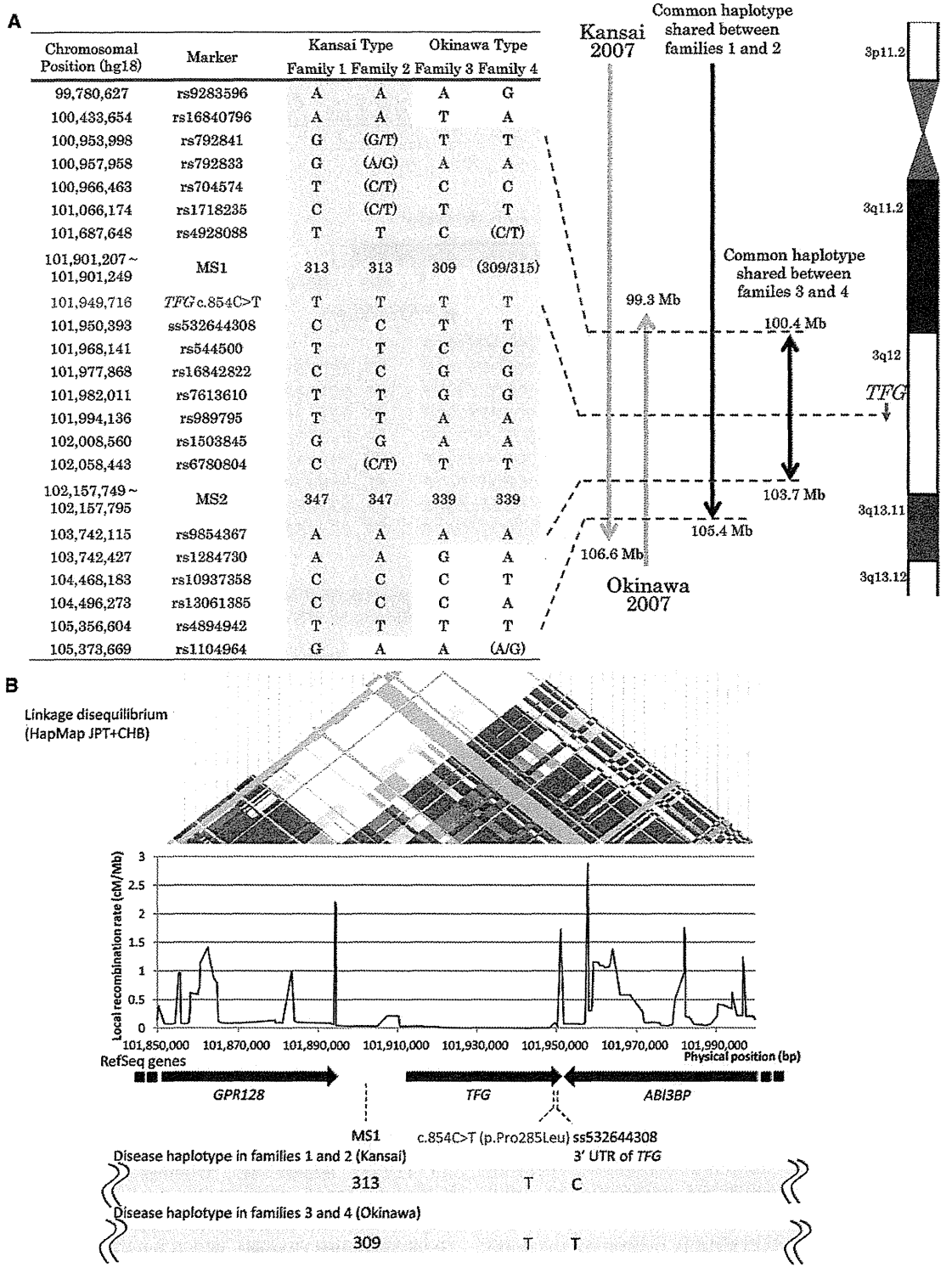

Figure 2. Haplotype Analysis and Minimum Candidate Region of HMSN-P
(A) Haplotypes were reconstructed for all the families with the use of SNP array data and microsatellite markers. Previously reported candidate regions are shown as "Kansai 2007" and "Okinawa 2007."[1,6] Because families 1 and 2 are distantly related, an extended shared common haplotype was observed on chromosome 3, as indicated by a previous study.[6] A reassessment of linkage analysis with high-density SNP markers revealed a recombination between rs4894942 and rs1104964 in family 2, thus refining the telomeric boundary of the candidate region in Kansai families (designated as "Common haplotype shared between families 1 and 2). Furthermore, a shared common haplotype (3.3 Mb with boundaries at rs16840796 and rs1284730) between families 3 and 4 was found, defining the minimum candidate region.

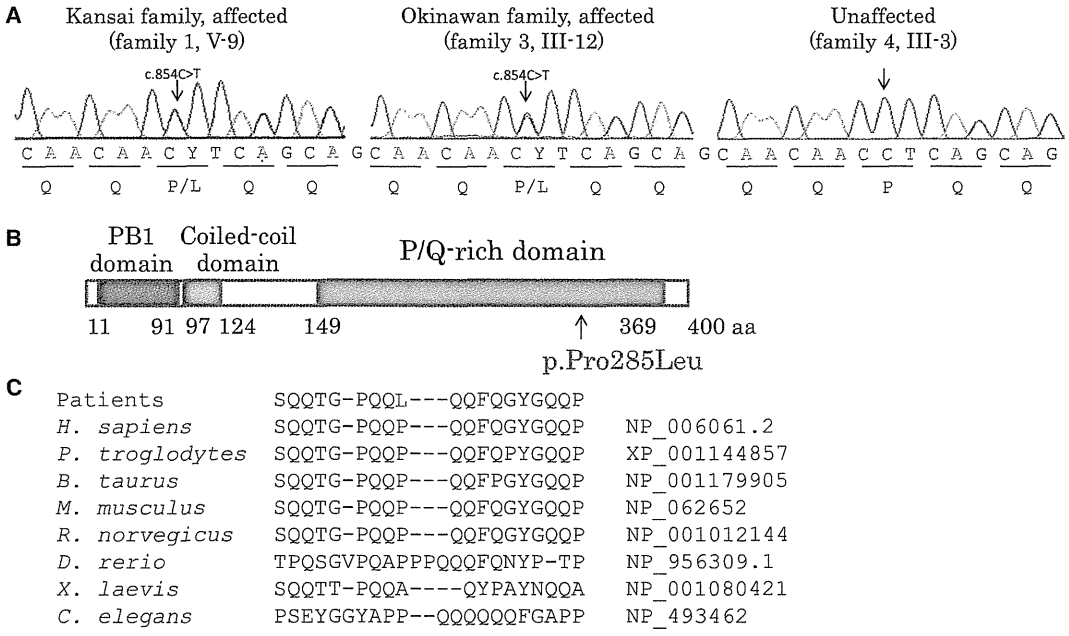

Figure 3. Identification of Causative Mutation
(A) Exome sequencing revealed that only one novel nonsynonymous variant is located within the minimum candidate region. Direct nucleotide-sequence analysis confirmed the mutation, c.854C>T (p.Pro285Leu), in *TFG* in both Kansai and Okinawan families. The mutation cosegregated with the disease (Figure 1A).
(B) Schematic representation of TFG isoform 1. The alteration (p.Pro285Leu) detected in this study is shown below.
(C) Cross-species homology search of the partial TFG amino acid sequence containing the p.Pro285Leu alteration revealed that Pro285 is evolutionally conserved among species.

pneumonia at 67 years of age.[5] Immunohistochemical observations employing a TFG antibody (Table S8) revealed fine granular immunostaining of TFG in the cytoplasm of motor neurons in the spinal cord of neurologically normal controls (n = 3; age at death = 58.7 ± 19.6 years old) (Figure 4A). In the HMSN-P patient, in contrast, TFG-immunopositive inclusion bodies were detected in the motor neurons of the facial, hypoglossal, and abducens nuclei and the spinal cord, as well as in the sensory neurons of the dorsal root ganglia, but were not detected in glial cells (Figures 4B–4D). A small number of cortical neurons in the precentral gyrus also showed TFG-immunopositive inclusion bodies (Figure 4E). Serial sections stained with antibodies against ubiquitin or TFG (Figure 4F) and double immunofluorescence staining (Figure 4G) demonstrated that TFG-immunopositive inclusions colocalized with ubiquitin deposition. Inclusion bodies were immunopositive for optineurin in motor neurons of the brainstem nuclei and the anterior horn of the spinal cord,[5] as well as in sensory neurons of the dorsal root ganglia (data not shown). These data strongly indicate that HMSN-P is a proteinopathy involving TFG.

Because HMSN-P and ALS share some clinical characteristics, we then examined whether neuropathological findings of HMSN-P shared cardinal features with those of sporadic ALS.[13–16] Immunohistochemistry with a TDP-43 antibody revealed skein-like inclusions in the remaining motor neurons of the abducens nucleus and the anterior horn of the lumbar cord (Figures 4H–4I). Phosphorylated TDP-43-positive inclusions were also identified in neurons of the anterior horn of the cervical cord and Clarke's nucleus (Figures 4J–4K). In contrast, TFG immunostaining of spinal-cord specimens from four patients with sporadic ALS (their age at death was 72.3 ± 7.4 years old) revealed no pathological staining in the motor neurons (data not shown). Double immunofluorescence staining revealed that many of the TFG-immunopositive round inclusions in the HSMN-P patient were negative for TDP-43 (Figure 4L), whereas a small number of inclusions were positive for both TFG and TDP-43 (Figure 4M). In addition, to investigate morphological Golgi-apparatus changes, which have recently been found in motor neurons of autopsied tissues of ALS patients,[17] we conducted immunohistochemical analysis by using

(B) Disease haplotypes in the Kansai and Okinawan kindreds are indicated below. Local recombination rates, RefSeq genes, and the linkage disequilibrium map from HapMap JPT (Japanese in Tokyo, Japan) and CHB (Han Chinese in Beijing, China) samples are shown above the disease haplotypes. When disease haplotypes of the Kansai and Okinawan kindreds are compared, the markers nearest to *TFG* are discordant at markers 48.5 kb centromeric and 677 bp telomeric to the mutation within a haploblock, strongly supporting the interpretation that the mutations have independent origins.

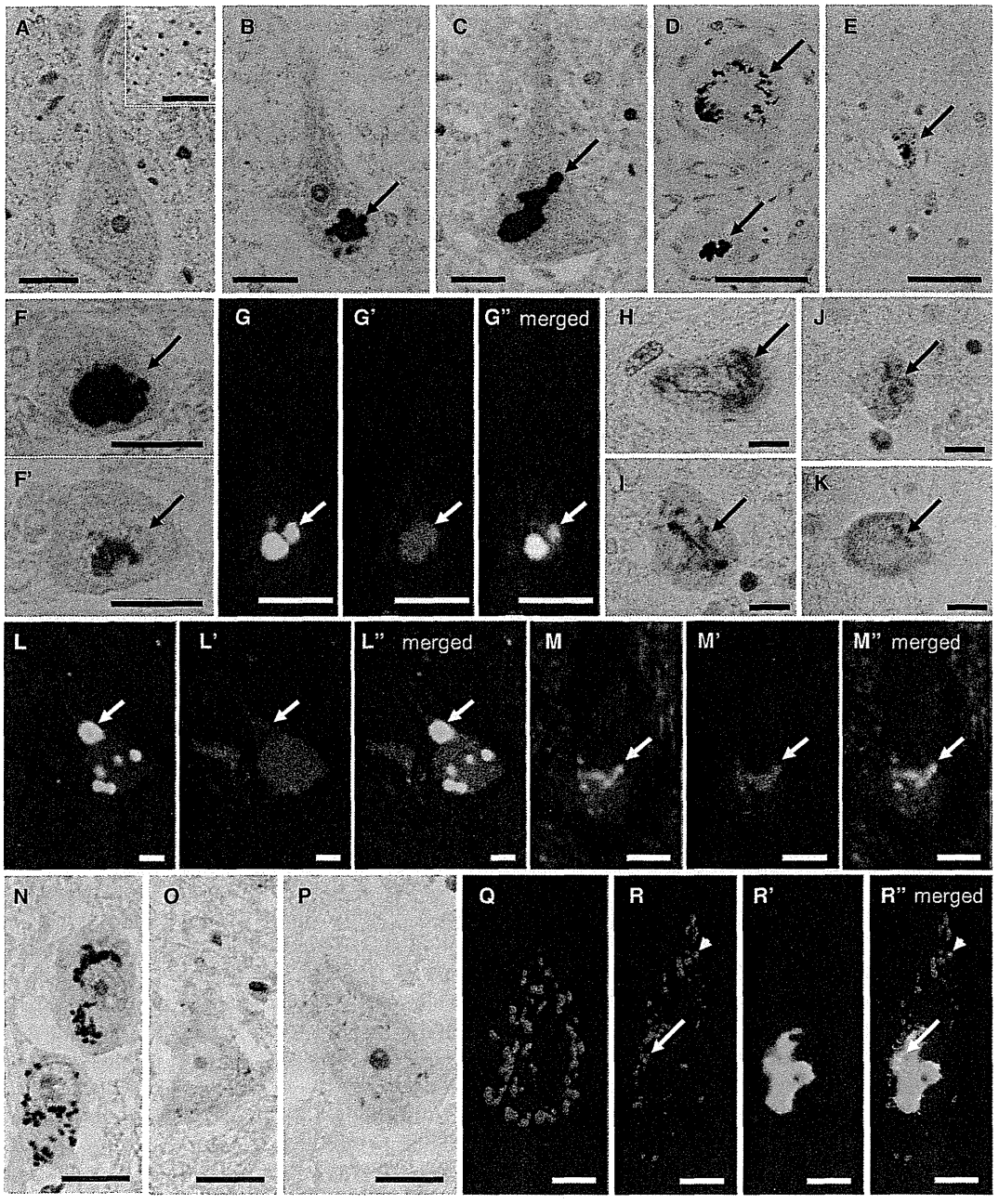

Figure 4. TFG-Related Neuropathological Findings

(A) TFG immunostaining (with hematoxylin counterstaining) of a motor neuron in the spinal cord of a neurologically normal control. A high-power magnified photomicrograph (inset) shows fine granular staining of TFG in the cytoplasm. The scale bars represent 20 μm (main panel) and 10 μm (inset).

(B–E) TFG-immunopositive inclusions of the neurons (with hematoxylin counterstaining) in the hypoglossal nucleus (B), anterior horn of the spinal cord (C), dorsal root ganglion (D, arrows), and motor cortex (E, arrow) of the patient with the *TFG* mutation. The scale bars represent 20 μm (B–D) and 50 μm (E).

(F and F′) Serial section analysis of the facial nucleus motor neuron showing an inclusion body colabeled for TFG (F) and ubiquitin (F′). The scale bars represent 20 μm.

(G–G″) Double immunofluorescence microscopy confirming colocalization of TFG (green) and ubiquitin (red) in an inclusion body of a motor neuron in the hypoglossal nucleus. The scale bars represent 20 μm.

(H and I) TDP-43-positive skein-like inclusions in the motor neurons of the abducens nucleus (H) and anterior horn of the lumbar cord (I). The scale bars represent 20 μm.

(J and K) Phosporylated TDP-43-positive inclusion bodies in the cervical anterior horn (J) and Clarke's nucleus (K). The scale bars represent 20 μm.

(L–L″) Round inclusions (arrows) positive for TFG (green) but negative for TDP-43 (red). The scale bars represent 20 μm.

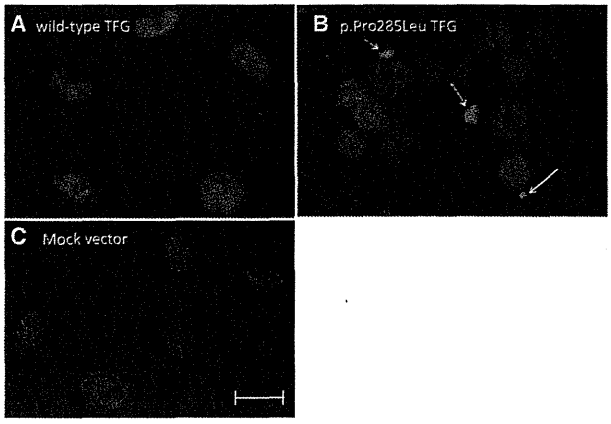

Figure 5. Formation of Cytoplasmic TDP-43 Aggregation Bodies in Cells Stably Expressing Mutant p.Pro285Leu TFG
The coding sequence of *TFG* cDNA was subcloned into pBluescript (Stratagene). After site-directed mutagenesis with a primer pair shown in Table S9, the mutant cDNAs were cloned into the BamHI and XhoI sites of pcDNA3 (Life Technologies). Stable cell lines were established by Lipofectamine (Life Technologies) transfection according to the manufacturer's instructions. Established cell lines were cultured under the ordinary cell-culture conditions (37°C and 5% CO_2) for 5–6 days and were subjected to immunocytochemical analyses. Neuro-2a cells stably expressing wild-type TFG (A), mutant TFG (p.Pro285Leu) (B), and a mock vector (C) are shown. TDP-43-immunopositive cytoplasmic inclusions are absent in the cells stably expressing wild-type TFG or the mock vector (A and C); however, TDP-43-immunopositive cytoplasmic inclusions were exclusively demonstrated in cells stably expressing mutant TFG (p.Pro285Leu), as indicated by arrows (B). Similar results were obtained with HEK 293 cells (not shown). Scale bars represent 10 μm.

a TGN46 antibody. It revealed that the Golgi apparatus was fragmented in approximately 70% of the remaining motor neurons in the lumbar anterior horn. The fragmentation of the Golgi apparatus was prominent near TFG-positive inclusion bodies (Figures 4N–4R). In summary, we found abnormal TDP-43-immunopositive inclusions in the cytoplasm of motor neurons, as well as fragmentation of the Golgi apparatus in HMSN-P, confirming the overlapping neuropathological features between HMSN-P and sporadic ALS.

To further investigate the effect of mutant TFG in cultured cells, stable cell lines expressing wild-type and mutant TFG (p.Pro285Leu) were established from neuro-2a and human embryonic kidney (HEK) 293 cells as previously described.[18] Established cell lines were cultured under the ordinary cell-culture conditions (37°C and 5% CO_2) for 5–6 days and were subjected to immunocytochemical analyses. The neuro-2a cells stably expressing wild-type or mutant TFG demonstrated no distinct difference in the distribution of endogenous TFG, FUS, or OPTN (data not shown). In contrast, cytoplasmic inclusions containing endogenous TDP-43 were exclusively observed in the neuro-2a cells stably expressing untagged mutant TFG, but not in those expressing wild-type TFG (Figure 5). Similar data were obtained from HEK 293 cells (data not shown). Thus, the expression of mutant TFG leads to mislocalization and inclusion-body formation of TDP-43 in cultured cells.

TFG was originally identified as a part of fusion oncoproteins (NTRK1-T3 in papillary thyroid carcinoma,[19] TFG-ALK in anaplastic large cell lymphoma,[20] and TFG/NOR1 in extraskeletal myxoid chondrosarcoma[21]), where the N-terminal portions of TFG are fused to the C terminus of tyrosine kinases or a superfamily of steroid-thyroid hormone-retinoid receptors acting as a transcriptional activator leading to the formation of oncogenic products. Very recently, TFG-1, a homolog of TFG in *Caenorhabditis elegans*, and TFG have been discovered to localize in endoplasmic-reticulum exit sites. TFG-1 acts in a hexameric form that binds the scaffolding protein Sec16 complex assembly and plays an important role in protein secretion with COPII-coated vesicles.[22] It is noteworthy that mutations in genes involved in vesicle trafficking[23,24] (such genes include *VAPB*, *CHMP2B*, *alsin*, *FIG4*, *VPS33B*, *PIP5K1C*, and *ERBB3*) cause motor neuron diseases, emphasizing the role of vesicle trafficking in motor neuron diseases. Thus, altered vesicle trafficking due to the *TFG* mutation might be involved in the motor neuron degeneration in HMSN-P. The presence of TFG-immunopositive inclusions in motor neurons raises the possibility that mutant TFG results in the misfolding and formation of cytoplasmic aggregate bodies, as well as altered vesicle trafficking.

An intriguing neuropathological finding is TDP-43-positive cytoplasmic inclusions in the motor neurons; these inclusions have recently been established as the fundamental neuropathological findings in ALS.[13,14] Of note, expression of mutant, but not wild-type, TFG in cultured cells led to the formation of TDP-43-containing cytoplasmic aggregation. These observations are similar

(M–M″) An inclusion immunopositive for both TFG (green) and TDP-43 (red) is observed in a small number of neurons. The scale bars represent 20 μm.
(N) Normal Golgi apparatus in the neurons of the intact thoracic intermediolateral nucleus. The scale bar represents 20 μm.
(O and P) Fragmentation of the Golgi apparatus with small, round, and disconnected profiles in the affected motor neurons of the lumbar anterior horn. The scale bars represent 20 μm.
(Q–R″) Immunohistochemical observations of the Golgi apparatus and TFG-immunopositive inclusions employing antibodies against TGN46 (red) and TFG (green), respectively. The scale bars represent 10 μm.
(Q) Normal size and distribution (red) in a motor neuron without inclusions.
(R–R″) The Golgi apparatus was fragmented into various sizes and reduced in number in the lumbar anterior horn motor neuron with TFG-positive inclusions (green). The fragmentation predominates near the inclusion (arrow), whereas the Golgi apparatuses distant from the inclusion showed nearly normal patterns (arrow head).

to what has been described for ALS, where TDP-43 is mislocalized from the normally localized nucleus to the cytoplasm with concomitant cytoplasmic inclusions. Cytoplasmic TDP-43 accumulation and inclusion formation have also been observed in motor neurons in familial ALS with mutations in *VAPB* (MIM 608627) or *CHMP2B* (MIM 600795).[25,26] Furthermore, TDP-43 pathology has been demonstrated in transgenic mice expressing mutant VAPB.[27] Although the mechanisms of mislocalization of TDP-43 remain to be elucidated, these observations suggest connections between alteration of vesicle trafficking and mislocalization of TDP-43. Thus, common pathophysiologic mechanisms might underlie motor neuron degenerations involving vesicle trafficking including TFG, as well as VAPB and CHMP2B. Because TDP-43 is an RNA-binding protein, RNA dysregulation has been suggested to play important roles in the TDP43-mediated neurodegeneration.[28] Furthermore, recent discovery of hexanucleotide repeat expansions in *C9ORF72* in familial and sporadic ALS/FTD (MIM 105550)[29,30] emphasizes the RNA-mediated toxicities as the causal mechanisms of neurodegeneration. Observations of TDP-43-positive cytoplasmic inclusions in the motor neurons of the patient with HMSN-P raise the possibility that RNA-mediated mechanisms might also be involved in motor neuron degeneration in HMSN-P.

In summary, we have found that *TFG* mutations cause HMSN-P. The presence of TFG/ubiquitin- and/or TDP-43-immunopositive cytoplasmic inclusions in motor neurons and cytosolic aggregation composed of TDP-43 in cultured cells expressing mutant TFG indicate a novel pathway of motor neuron death.

Supplemental Data

Supplemental Data include three figures and nine tables and can be found with this article online at http://www.cell.com/AJHG/.

Acknowledgments

The authors thank the families for participating in the study. We also thank the doctors who obtained clinical information of the patients. This work was supported in part by Grants-in-Aid for Scientific Research on Innovative Areas (22129002); the Global Centers of Excellence Program; the Integrated Database Project; Scientific Research (A) (B21406026) and Challenging Exploratory Research (23659458) from the Ministry of Education, Culture, Sports, Science, and Technology of Japan; a Grant-in-Aid for Research on Intractable Diseases and Comprehensive Research on Disability Health and Welfare from the Ministry of Health, Labour, and Welfare, Japan; Grants-in-Aid from the Research Committee of CNS Degenerative Diseases; the Ministry of Health, Labour, and Welfare of Japan; the Charcot-Marie-Tooth Association; and the National Medical Research Council of Australia. H.I. was supported by a Research Fellowship from the Japan Society for the Promotion of Science for Young Scientists. We also thank S. Ogawa (Cancer Genomics Project, The University of Tokyo) for his kind help in the analyses employing GAIIx and SOLiD4.

Received: April 16, 2012
Revised: May 27, 2012
Accepted: July 2, 2012
Published online: August 9, 2012

Web Resources

The URLs for data presented herein are as follows.

1000 Genomes Project Database, http://www.1000genomes.org/
dbSNP, http://www.ncbi.nlm.nih.gov/projects/SNP/
HapMap, http://hapmap.ncbi.nlm.nih.gov/
NHLBI GO Exome Sequencing Project, https://esp.gs.washington.edu/drupal/
Online Mendelian Inheritance in Man (OMIM), http://www.omim.org
PolyPhen, http://genetics.bwh.harvard.edu/pph/
RefSeq, http://www.ncbi.nlm.nih.gov/projects/RefSeq/
UCSC Human Genome Browser, http://genome.ucsc.edu/

References

1. Takashima, H., Nakagawa, M., Nakahara, K., Suehara, M., Matsuzaki, T., Higuchi, I., Higa, H., Arimura, K., Iwamasa, T., Izumo, S., and Osame, M. (1997). A new type of hereditary motor and sensory neuropathy linked to chromosome 3. Ann. Neurol. *41*, 771–780.
2. Nakagawa, M. (2009). [Wide spectrum of hereditary motor sensory neuropathy (HMSN)]. Rinsho Shinkeigaku *49*, 950–952.
3. Maeda, K., Sugiura, M., Kato, H., Sanada, M., Kawai, H., and Yasuda, H. (2007). Hereditary motor and sensory neuropathy (proximal dominant form, HMSN-P) among Brazilians of Japanese ancestry. Clin. Neurol. Neurosurg. *109*, 830–832.
4. Patroclo, C.B., Lino, A.M., Marchiori, P.E., Brotto, M.W., and Hirata, M.T. (2009). Autosomal dominant HMSN with proximal involvement: new Brazilian cases. Arq. Neuropsiquiatr. *67* (3B), 892–896.
5. Fujita, K., Yoshida, M., Sako, W., Maeda, K., Hashizume, Y., Goto, S., Sobue, G., Izumi, Y., and Kaji, R. (2011). Brainstem and spinal cord motor neuron involvement with optineurin inclusions in proximal-dominant hereditary motor and sensory neuropathy. J. Neurol. Neurosurg. Psychiatry *82*, 1402–1403.
6. Takahashi, H., Makifuchi, T., Nakano, R., Sato, S., Inuzuka, T., Sakimura, K., Mishina, M., Honma, Y., Tsuji, S., and Ikuta, F. (1994). Familial amyotrophic lateral sclerosis with a mutation in the Cu/Zn superoxide dismutase gene. Acta Neuropathol. *88*, 185–188.
7. Maeda, K., Kaji, R., Yasuno, K., Jambaldorj, J., Nodera, H., Takashima, H., Nakagawa, M., Makino, S., and Tamiya, G. (2007). Refinement of a locus for autosomal dominant hereditary motor and sensory neuropathy with proximal dominancy (HMSN-P) and genetic heterogeneity. J. Hum. Genet. *52*, 907–914.
8. Fukuda, Y., Nakahara, Y., Date, H., Takahashi, Y., Goto, J., Miyashita, A., Kuwano, R., Adachi, H., Nakamura, E., and Tsuji, S. (2009). SNP HiTLink: A high-throughput linkage analysis system employing dense SNP data. BMC Bioinformatics *10*, 121.
9. Gudbjartsson, D.F., Thorvaldsson, T., Kong, A., Gunnarsson, G., and Ingolfsdottir, A. (2005). Allegro version 2. Nat. Genet. *37*, 1015–1016.

10. Li, H., and Durbin, R. (2009). Fast and accurate short read alignment with Burrows-Wheeler transform. Bioinformatics *25*, 1754–1760.
11. Li, H., Handsaker, B., Wysoker, A., Fennell, T., Ruan, J., Homer, N., Marth, G., Abecasis, G., and Durbin, R.; 1000 Genome Project Data Processing Subgroup. (2009). The Sequence Alignment/Map format and SAMtools. Bioinformatics *25*, 2078–2079.
12. Robinson, J.T., Thorvaldsdóttir, H., Winckler, W., Guttman, M., Lander, E.S., Getz, G., and Mesirov, J.P. (2011). Integrative genomics viewer. Nat. Biotechnol. *29*, 24–26.
13. Neumann, M., Sampathu, D.M., Kwong, L.K., Truax, A.C., Micsenyi, M.C., Chou, T.T., Bruce, J., Schuck, T., Grossman, M., Clark, C.M., et al. (2006). Ubiquitinated TDP-43 in frontotemporal lobar degeneration and amyotrophic lateral sclerosis. Science *314*, 130–133.
14. Arai, T., Hasegawa, M., Akiyama, H., Ikeda, K., Nonaka, T., Mori, H., Mann, D., Tsuchiya, K., Yoshida, M., Hashizume, Y., and Oda, T. (2006). TDP-43 is a component of ubiquitin-positive tau-negative inclusions in frontotemporal lobar degeneration and amyotrophic lateral sclerosis. Biochem. Biophys. Res. Commun. *351*, 602–611.
15. Hasegawa, M., Arai, T., Nonaka, T., Kametani, F., Yoshida, M., Hashizume, Y., Beach, T.G., Buratti, E., Baralle, F., Morita, M., et al. (2008). Phosphorylated TDP-43 in frontotemporal lobar degeneration and amyotrophic lateral sclerosis. Ann. Neurol. *64*, 60–70.
16. Inukai, Y., Nonaka, T., Arai, T., Yoshida, M., Hashizume, Y., Beach, T.G., Buratti, E., Baralle, F.E., Akiyama, H., Hisanaga, S., and Hasegawa, M. (2008). Abnormal phosphorylation of Ser409/410 of TDP-43 in FTLD-U and ALS. FEBS Lett. *582*, 2899–2904.
17. Stieber, A., Chen, Y., Wei, S., Mourelatos, Z., Gonatas, J., Okamoto, K., and Gonatas, N.K. (1998). The fragmented neuronal Golgi apparatus in amyotrophic lateral sclerosis includes the trans-Golgi-network: Functional implications. Acta Neuropathol. *95*, 245–253.
18. Kuroda, Y., Sako, W., Goto, S., Sawada, T., Uchida, D., Izumi, Y., Takahashi, T., Kagawa, N., Matsumoto, M., Matsumoto, M., et al. (2012). Parkin interacts with Klokin1 for mitochondrial import and maintenance of membrane potential. Hum. Mol. Genet. *21*, 991–1003.
19. Greco, A., Mariani, C., Miranda, C., Lupas, A., Pagliardini, S., Pomati, M., and Pierotti, M.A. (1995). The DNA rearrangement that generates the TRK-T3 oncogene involves a novel gene on chromosome 3 whose product has a potential coiled-coil domain. Mol. Cell. Biol. *15*, 6118–6127.
20. Hernández, L., Pinyol, M., Hernández, S., Beà, S., Pulford, K., Rosenwald, A., Lamant, L., Falini, B., Ott, G., Mason, D.Y., et al. (1999). TRK-fused gene (TFG) is a new partner of ALK in anaplastic large cell lymphoma producing two structurally different TFG-ALK translocations. Blood *94*, 3265–3268.
21. Hisaoka, M., Ishida, T., Imamura, T., and Hashimoto, H. (2004). TFG is a novel fusion partner of NOR1 in extraskeletal myxoid chondrosarcoma. Genes Chromosomes Cancer *40*, 325–328.
22. Witte, K., Schuh, A.L., Hegermann, J., Sarkeshik, A., Mayers, J.R., Schwarze, K., Yates, J.R., 3rd, Eimer, S., and Audhya, A. (2011). TFG-1 function in protein secretion and oncogenesis. Nat. Cell Biol. *13*, 550–558.
23. Dion, P.A., Daoud, H., and Rouleau, G.A. (2009). Genetics of motor neuron disorders: New insights into pathogenic mechanisms. Nat. Rev. Genet. *10*, 769–782.
24. Andersen, P.M., and Al-Chalabi, A. (2011). Clinical genetics of amyotrophic lateral sclerosis: What do we really know? Nat Rev Neurol *7*, 603–615.
25. Ince, P.G., Highley, J.R., Kirby, J., Wharton, S.B., Takahashi, H., Strong, M.J., and Shaw, P.J. (2011). Molecular pathology and genetic advances in amyotrophic lateral sclerosis: an emerging molecular pathway and the significance of glial pathology. Acta Neuropathol. *122*, 657–671.
26. Cox, L.E., Ferraiuolo, L., Goodall, E.F., Heath, P.R., Higginbottom, A., Mortiboys, H., Hollinger, H.C., Hartley, J.A., Brockington, A., Burness, C.E., et al. (2010). Mutations in CHMP2B in lower motor neuron predominant amyotrophic lateral sclerosis (ALS). PLoS ONE *5*, e9872.
27. Tudor, E.L., Galtrey, C.M., Perkinton, M.S., Lau, K.-F., De Vos, K.J., Mitchell, J.C., Ackerley, S., Hortobágyi, T., Vámos, E., Leigh, P.N., et al. (2010). Amyotrophic lateral sclerosis mutant vesicle-associated membrane protein-associated protein-B transgenic mice develop TAR-DNA-binding protein-43 pathology. Neuroscience *167*, 774–785.
28. Lee, E.B., Lee, V.M., and Trojanowski, J.Q. (2012). Gains or losses: Molecular mechanisms of TDP43-mediated neurodegeneration. Nat. Rev. Neurosci. *13*, 38–50.
29. DeJesus-Hernandez, M., Mackenzie, I.R., Boeve, B.F., Boxer, A.L., Baker, M., Rutherford, N.J., Nicholson, A.M., Finch, N.A., Flynn, H., Adamson, J., et al. (2011). Expanded GGGGCC hexanucleotide repeat in noncoding region of C9ORF72 causes chromosome 9p-linked FTD and ALS. Neuron *72*, 245–256.
30. Renton, A.E., Majounie, E., Waite, A., Simón-Sánchez, J., Rollinson, S., Gibbs, J.R., Schymick, J.C., Laaksovirta, H., van Swieten, J.C., Myllykangas, L., et al; ITALSGEN Consortium. (2011). A hexanucleotide repeat expansion in C9ORF72 is the cause of chromosome 9p21-linked ALS-FTD. Neuron *72*, 257–268.

EMBO
Molecular Medicine

Altered γ-secretase activity in mild cognitive impairment and Alzheimer's disease

Nobuto Kakuda[1,2,3], Mikio Shoji[4], Hiroyuki Arai[5], Katsutoshi Furukawa[5], Takeshi Ikeuchi[6], Kohei Akazawa[7], Mako Takami[2,3], Hiroyuki Hatsuta[8], Shigeo Murayama[8], Yasuhiro Hashimoto[9], Masakazu Miyajima[10], Hajime Arai[10], Yu Nagashima[11], Haruyasu Yamaguchi[12], Ryozo Kuwano[13], Kazuhiro Nagaike[1], Yasuo Ihara[2,14,3], the Japanese Alzheimer's Disease Neuroimaging Initiative*

Keywords: amyloid β-protein; CSF; γ-secretase; NSAID; stepwise processing

DOI 10.1002/emmm.201200214

Received December 21, 2010
Revised December 22, 2011
Accepted January 09, 2012

We investigated why the cerebrospinal fluid (CSF) concentrations of Aβ42 are lower in mild cognitive impairment (MCI) and Alzheimer's disease (AD) patients. Because Aβ38/42 and Aβ40/43 are distinct product/precursor pairs, these four species in the CSF together should faithfully reflect the status of brain γ-secretase activity, and were quantified by specific enzyme-linked immunosorbent assays in the CSF from controls and MCI/AD patients. Decreases in the levels of the precursors, Aβ42 and 43, in MCI/AD CSF tended to accompany increases in the levels of the products, Aβ38 and 40, respectively. The ratios Aβ40/43 *versus* Aβ38/42 in CSF (each representing cleavage efficiency of Aβ43 or Aβ42) were largely proportional to each other but generally higher in MCI/AD patients compared to control subjects. These data suggest that γ-secretase activity in MCI/AD patients is enhanced at the conversion of Aβ43 and 42 to Aβ40 and 38, respectively. Consequently, we measured the *in vitro* activity of raft-associated γ-secretase isolated from control as well as MCI/AD brains and found the same, significant alterations in the γ-secretase activity in MCI/AD brains.

INTRODUCTION

Senile plaques, the neuropathological hallmark of Alzheimer's disease (AD), are composed of amyloid β-protein (Aβ). Aβ is derived from β-amyloid precursor protein (APP) through sequential cleavage by β- and γ-secretases. β-Secretase cleaves at the luminal portion (β-site) of APP to generate a β-carboxyl terminal fragment of APP (βCTF), an immediate substrate of γ-secretase, to produce different Aβ species (for a review see Selkoe, 2001). The most abundant secreted Aβ species is Aβ40,

(1) Immuno-Biological Laboratories Co., Fujioka, Japan
(2) Faculty of Life and Medical Sciences, Department of Neuropathology, Doshisha University, Kyoto, Japan
(3) New Energy and Industrial Technology Development Organization (NEDO), Kanagawa, Japan
(4) Department of Neurology, Institute of Brain Science, Hirosaki University Graduate School of Medicine, Hirosaki, Japan
(5) Division of Brain Sciences, Department of Geriatrics and Gerontology, Institute of Development, Aging and Cancer, Tohoku University, Sendai, Japan
(6) Department of Neurology, Brain Research Institute, Niigata University, Niigata, Japan
(7) Department of Medical Informatics, Niigata University Medical and Dental Hospital, Niigata, Japan
(8) Department of Neuropathology, Tokyo Metropolitan Institute of Gerontology, Tokyo, Japan
(9) Department of Biochemistry, Fukushima Medical University, Fukushima, Japan
(10) Department of Neurosurgery, Juntendo University School of Medicine, Tokyo, Japan
(11) Department of Neurology, Graduate School of Medicine, University of Tokyo, Tokyo, Japan
(12) Gunma University School of Health Sciences, Maebashi, Japan
(13) Department of Molecular Genetics, Bioresource Science Branch, Center for Bioresources, Niigata University, Niigata, Japan
(14) Core Research for Evolutional Science and Technology (CREST), Japan Science and Technology Corporation, Tokyo, Japan
***Corresponding author:** Tel: +81 774 656058; Fax: +81 774 731922;
E-mail: yihara@mail.doshisha.ac.jp

whereas the species that has two extra residues (Aβ42) is a minor one (<10%); however, the latter is the one that deposits first and predominates in senile plaques (Iwatsubo et al, 1994).

Presenilin 1/2 make up the catalytic site of γ-secretase. The enzymatic properties of γ-secretase that cleave the transmembrane domain of βCTF have been an enigma, although recent studies provided partial elucidation of this mechanism (Qi-Takahara et al, 2005; Takami et al, 2009). γ-Secretase has two product lines, which successively convert the Aβ49 and Aβ48 that are generated by ε-cleavage, to shorter Aβs by releasing tri- or tetrapeptides in a stepwise fashion. Aβ49 is successively cleaved mostly into Aβ40 via Aβ46 and Aβ43, while Aβ48 is similarly cleaved into Aβ38 via Aβ45 and Aβ42 (see Fig 1). Importantly, the differences between the amounts of released tri- and tetrapeptides determine the levels of the different Aβ species produced (Takami et al, 2009). Thus, the true activity of γ-secretase is defined by the amounts of tri- and tetrapeptides released, but not by the amounts of Aβ species produced. Of note, the most abundant species Aβ40 is derived not from Aβ42, but from Aβ43. Also Aβ38 is derived mainly from Aβ42 (Fig 1). The longer Aβs in cerebrospinal fluid (CSF) including Aβ49 and 46 as well as Aβ48 and 45 must be generated at negligible levels, but may neither be secreted to the interstitial fluid (ISF) nor recruited to CSF. This suggests that the status of brain, and possibly neuronal, γ-secretase could be accurately assessed by measuring all four Aβ species generated by the two product lines of γ-secretase.

Using enzyme-linked immunosorbent assays (ELISAs), we quantified Aβ40 and 43 and Aβ38 and 42 in CSF samples from control subjects and mild cognitive impairment (MCI)/AD patients. The CSF concentrations of Aβ43 and Aβ42 were found to be significantly lower in MCI/AD compared with controls. The ratio of Aβ38/42, which represents the ratio of product/precursor and thus the cleavage efficiency of Aβ42, was plotted against the ratio of Aβ40/43, which represents the ratio of product/precursor in the other product line and thus the cleavage efficiency of Aβ43. The ratio of Aβ38/42 was largely proportional to that of Aβ40/43, indicating that the two cleavage processes are tightly coupled, but both were generally higher in MCI/AD patients compared to control subjects These results

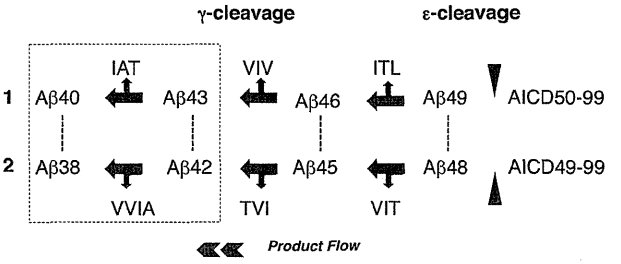

Figure 1. Generation of Aβs through stepwise processing of βCTF. At the first step, βCTF is cleaved at the membrane-cytoplasmic boundary (ε-cleavage), producing AICD (APP intracellular domain) 50–99 and 49–99. Counterparts Aβ49 and 48 in turn are cleaved in a stepwise fashion, releasing tri- and tetrapeptides. One product line converts Aβ49 mostly to Aβ40 via Aβ46 and Aβ43. The other product line converts Aβ48 to Aβ38 via Aβ45 and Aβ42. It should be noted that the differences between the amounts of released tri- or tetrapeptide determine the amounts of Aβs produced. Broken lines indicate corresponding Aβs on the two product lines.

suggest that the activity of brain γ-secretase in MCI/AD is enhanced at the conversion of Aβ43 to Aβ40 and Aβ42 to Aβ38, which would result in significantly lower CSF concentrations of Aβ42 and 43. In support of this hypothesis, the activities of raft-associated γ-secretase from control and MCI/AD brains were found to be significantly different: although the total Aβ production was similar, the γ-secretase in MCI/AD brains produced significantly larger ratios of Aβ40/43 and Aβ38/42 than the enzyme in control brains. This raises the possibility that lower CSF levels of Aβ42 and 43 simply reflect the altered γ-secretase activity in the MCI/AD-affected brains.

RESULTS

The CSF concentrations of Aβs were in the following order: Aβ40 > Aβ38 > Aβ42 ≫ Aβ43 in all CSF samples examined (Table 1 and Supporting Information Fig S2A). The relative amounts of Aβs were constant across the samples: Aβ38:40 ratio in CSF was ~1:3, and Aβ42:43 ratio was ~10:1. The CSF

Table 1. Subject characteristics and CSF concentrations of Aβs

	Control	MCI	AD	ANOVA ***p-value
Age (years)	74.9 ± 7.5	72.5 ± 6.6	72.3 ± 8.2	
N (male/female)	21 (10/11)	19 (7/12)	24 (7/17)	
MMSE score	28.7 ± 1.9	25.7 ± 2.6	19.6 ± 3.3	
ApoE ε4	3 (14.3%)	10 (52.6%) [a]	14 (58.6%) [a]	
Aβ38 (pM)	594.5 ± 286.3	669.4 ± 247.6	760.57 ± 269.4	
Ln(Aβ38)	6.28 ± 0.46	6.44 ± 0.38	6.56 ± 0.41	NS
Aβ40 (pM)	1607.9 ± 712.9	1939.5 ± 698.0	2292.6 ± 799.6	
Ln(Aβ40)	7.28 ± 0.47	7.51 ± 0.38	7.68 ± 0.35	0.007
Aβ42 (pM)	133.1 ± 53.4	83.2 ± 49.4**	90.3 ± 40.1 [a]	
Ln(Aβ42)	4.80 ± 0.47	4.25 ± 0.60	4.40 ± 0.47	0.004
Aβ43 (pM)	11.8 ± 5.7	6.8 ± 5.6**	7.0 ± 4.6**	
Ln(Aβ43)	2.32 ± 0.60	1.59 ± 0.86	1.76 ± 0.62	0.004

[a]2 MCI subjects were homozygous for ε4, while 4 AD subjects were homozygous for the allele.
**$p < 0.05$; Dunnett's *t*-test after log-transformation for comparing between control and MCI or AD.
***p-value of analysis of variance after log-transformation.

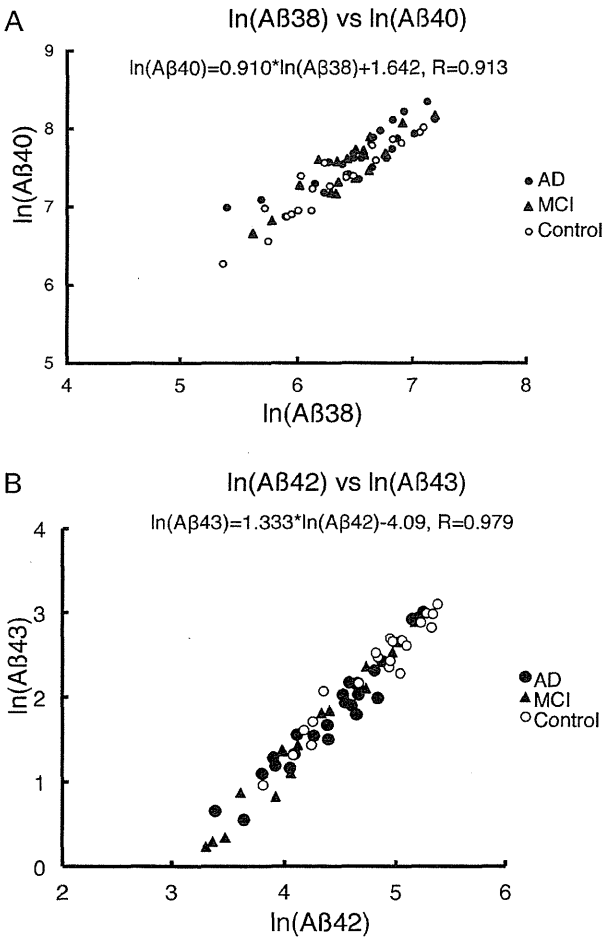

Figure 2. Relationships between the levels of Aβ40 and 38, and between those of Aβ43 and 42 in CSF from controls and MCI/AD patients.

A. The levels of ln(Aβ40) were proportional to those of ln(Aβ38) ($\ln(A\beta40) = 0.910 \times \ln(A\beta38) + 1.642$, $R = 0.913$).

B. The levels of ln(Aβ43) were proportional to those of ln(Aβ42) ($\ln(A\beta43) = 1.333 \times \ln(A\beta42) - 4.09$, $R = 0.979$). It should be noted that the levels of both ln(Aβ42) and ln(Aβ43) in MCI [filled triangle ($n = 19$)]/AD [filled circle ($n = 24$)] are lower than those in controls [open circles ($n = 21$)].

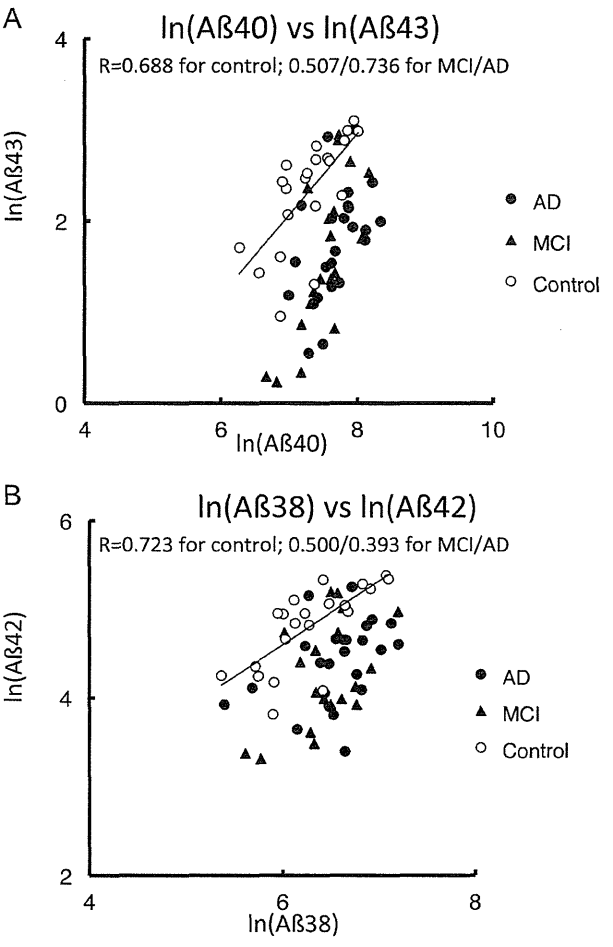

Figure 3. Relationships between the levels of Aβ43 and 40, and between those of Aβ42 and 38 in CSF from controls (open circles) and MCI (closed triangle)/AD patients (closed circle).

A. The levels of ln(Aβ43) correlate with those of ln(Aβ40) within controls ($R = 0.688$), and barely within MCI/AD subjects ($R = 0.507/0.736$). The plots for MCI/AD were located below the regression line for control ($p < 0.001$, ANOVA).

B. The levels of Aβ42 correlate with those of Aβ38 within controls ($R = 0.723$), and barely within MCI/AD ($R = 0.500/0.393$). The plots for MCI/AD were situated below the regression line for controls ($p < 0.001$, ANOVA).

concentrations of Aβ40 were significantly increased in AD compared to control (Table 1; $p < 0.05$, Dunnett's t-test). Additionally, the CSF concentrations of Aβ38 tended to be increased in AD patients compared to controls. In contrast, those of Aβ42 and 43 were significantly decreased in MCI/AD compared to controls ($p < 0.05$, Dunnett's t-test). Interestingly, as reported previously (Schoonenboom et al, 2005), the CSF concentrations of Aβ40 and Aβ38 were proportional to each other in all subjects [Fig 2A; $\ln(A\beta40) = 0.910 \times \ln(A\beta38) + 1.642$, $R = 0.913$, where ln(Aβ40) is the logarithm of Aβ40], even in MCI/AD cases. This was despite the fact that these species are derived from and the final products of the two different product lines of γ-secretase activity (Fig 1; Takami et al, 2009). In other words, the amounts of products in the third step of cleavage were strictly proportional to each other across the product lines.

Aβ42 and Aβ43 are produced by the second cleavage step of each product line. Like Aβ40 and Aβ38, the CSF concentrations of Aβ42 and Aβ43 are also proportional to each other in controls and in MCI/AD patients [Fig 2B; $\ln(A\beta43) = 1.333 \times \ln(A\beta42) - 4.09$, $R = 0.979$]. On the other hand, the levels of Aβ43 and Aβ40 (a precursor and its product) were correlated in control [Fig 3A; $\ln(A\beta43) = 0.884 \times \ln(A\beta40) - 4.118$, $R = 0.688$] and in MCI/AD subjects ($R = 0.507/0.736$ for MCI/AD, respectively) but the MCI/AD values were located below the regression line for controls and thus provided lower Aβ43 measures compared with controls for a given Aβ40 measure (Fig 3A; $p < 0.001$, analysis of variance, ANOVA). Conversely,

for a given Aβ43 value, the plot provided a higher Aβ40 measure in MCI/AD cases. There was a similar situation for the levels of Aβ42 and Aβ38. The levels of Aβ42 and Aβ38 were correlated each other in control subjects [Fig 3B; $\ln(A\beta42) = 0.724 \times \ln(A\beta38) + 0.251$, $R = 0.723$], but barely in MCI/AD ($R = 0.500$ for MCI; 0.393 for AD), and the MCI/AD plots were situated below the regression line for controls ($p < 0.001$, ANOVA). For a given Aβ42 value, the plot provided a higher Aβ38 measure in MCI/AD compared with controls.

These lower concentrations of Aβ42 appeared to be compensated with higher concentrations of Aβ38 as the levels of $\ln(A\beta38 + A\beta42)$ did not vary even in MCI/AD ($p = 0.293$, ANOVA). Thus, this points to the possibility that more Aβ42 and Aβ43 are converted to Aβ38 and Aβ40, respectively, in MCI/AD brains. According to numerical simulation based on the stepwise processing model, as the levels of βCTF decline to null, the levels of Aβ43 and 42 decrease and the ratios of Aβ40/43 and Aβ38/42 increase (unpublished observation). However, this situation can be excluded as the mechanism for lower concentrations of Aβ42 and 43, because the levels of βCTF have never been reported to be reduced in AD brains nor in plaque-forming Tg2576 mice that show lower CSF Aβ42 concentrations (Kawarabayashi et al, 2001). Thus, it is reasonable to suspect that the final cleavage steps from Aβ43 mostly to 40 and from Aβ42 to 38 are significantly enhanced in parallel (increases in released tri- and tetrapeptides) in brains affected by MCI/AD compared with controls (Fig 1).

This relationship in γ-secretase cleavage becomes clearer by plotting the product/precursor ratio representing cleavage efficiency at the step from Aβ42 to 38 (Aβ38/42) against that representing the cleavage efficiency at the step from Aβ43 to 40 (Aβ40/43) (Fig 4). The 'apparent' cleavage efficiency of Aβ43 was approximately 40-fold larger than that of Aβ42. The two ratios in CSF samples from MCI/AD and control subjects were largely proportional to each other, indicating that the corresponding cleavage processes in the two lines are tightly coupled (Fig 4). All plots were situated on a distinct line [$\ln(A\beta38/42) = 0.748 \times \ln(A\beta40/43) - 2.244$, $R = 0.936$] and its close surroundings. An increase in the cleavage from Aβ43 to 40 (*i.e.* more Aβ43 is converted to Aβ40) accompanied an increase in the cleavage from Aβ42 to 38 and *vice versa*, although the mechanism underlying this coupling between the two product lines remains unknown. This reminds us of the 'NSAID effect' in the 3-([3-cholamidopropyl]dimetylammonio)-2-hydroxy-1-propanesulfonate (CHAPSO)-reconstituted γ-secretase system (Takami et al, 2009; Weggen et al, 2001) in which the addition of sulindac sulfide to the γ-secretase reaction mixture, as expected, significantly suppressed Aβ42 production and increased Aβ38 production presumably by increasing the amounts of released tetrapeptide (VVIA) (Takami et al, 2009) and other peptides.

Most importantly, this graph provides a clear distinction between the control and MCI/AD groups (Fig 4; Aβ40/43 for MCI/AD *vs.* control, $p = 0.000$; Aβ38/42 for MCI/AD *vs.* control, $p = 0.000$; ANOVA, followed by Dunnett's *t*-test). The control values plotted close to the origin, whereas those for MCI/AD patients were distant from the origin along the line [$\ln(A\beta38/42) = 0.748 \times \ln(A\beta40/43) - 2.244$, $R = 0.936$]. It is also of note

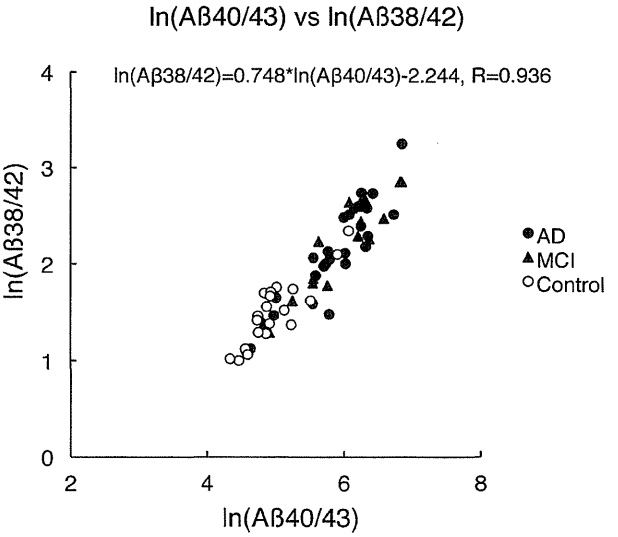

Figure 4. Ln(Aβ40/43) *versus* ln(Aβ38/42) plot. The ratios represent the cleavage efficiency at the final step of each line. Both ratios are largely proportional to each other ($y = 0.748 \times -2.244$, $R = 0.936$) and plots are located on the line and its close surroundings. This plot clearly distinguishes between control subjects and MCI/AD patients (Aβ40/43 for MCI *vs.* control, $p = 0.000$; Aβ38/42 for MCI *vs.* control, $p = 0.000$; ANOVA, followed by Dunnett's *t*-test). Control plots [open circles ($n = 21$)] are located close to the origin and MCI/AD plots [closed triangles ($n = 19$) and closed circles ($n = 24$), respectively] are a little distant from the origin.

that there was no significant difference between MCI and AD patients (Fig 4; Aβ40/43 for AD *vs.* MCI, $p = 1.000$; Aβ38/42 for AD *vs.* MCI, $p = 1.000$; Bonferroni's *t*-test). Two control values were a little farther from the origin, which may suggest that these subjects already have latent Aβ deposition or are in the preclinical AD stage. Additionally, we examined quite a small number of CSF samples from presenilin (PS) 1-mutated (symptomatic) familial AD (FAD) patients (T116N, L173F, G209R, L286V and L381V). Out of the three FAD cases near the regression line, two (T116N and L286V) were distant from the origin like sporadic AD cases and one (L381V) was closer to the origin than controls (both Aβ42/43 levels were lower than control; unpublished data). The remaining two (G209R and L173F) were extremely displaced from the line. Thus, a larger number of FAD cases are needed to give an appropriate explanation for their unusual characteristics in the plot, and the alteration of CSF Aβs shown above seems to be applicable only for sporadic AD.

Altogether, in MCI/AD, more Aβ42 and 43 are processed to Aβ38 and 40, respectively, than in controls. Even in MCI/AD, strict relationships are maintained between the levels of Aβ42 and Aβ43, and between those of Aβ38 and Aβ40 as seen in controls, which are predicted by the stepwise processing kinetics (unpublished observation). Thus, our observations suggest that lower CSF concentrations of Aβ42 and 43 and presumably higher CSF concentrations of Aβ38 and 40 are the consequence of altered γ-secretase activity in brain rather than the effect of preferential deposition of the two longer Aβ species (Aβ42 and 43) in senile plaques, which would not have maintained such strict relationships between the four Aβ species in CSF.

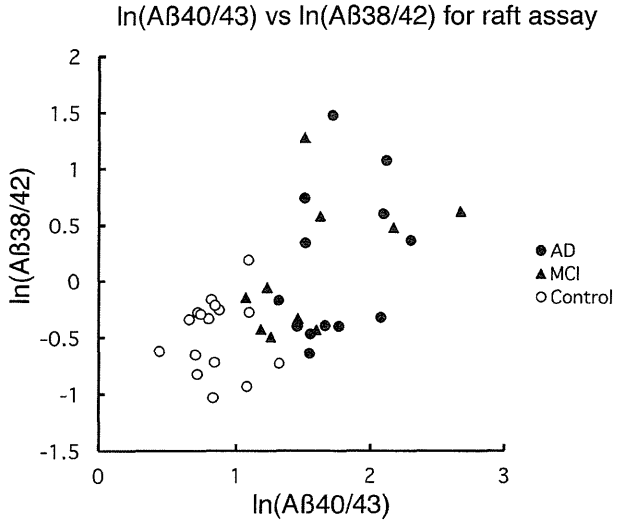

Figure 5. Ln(Aβ40/43) *versus* ln(Aβ38/42) plot based on direct quantification of raft-associated γ-secretase activity. The raft-associated γ-secretase prepared from control and MCI/AD brain specimens was incubated with βCTF for 2 h at 37°C (see Materials and Methods Section). Produced Aβs were quantified by Western blotting using specific antibodies. This plot distinguishes between control subjects and MCI/AD patients (Aβ40/43 for control *vs.* MCI/AD, $p < 0.001$; Aβ38/42 for control *vs.* MCI/AD, $p = 0.001$; Welch's *t*-test). MCI/AD plots [closed triangles ($n = 10$) and closed circles ($n = 13$), respectively] are as a whole a little distant from the origin, whereas control plots [open circles ($n = 16$)] are close to the origin.

To further test our hypothesis, we directly measured γ-secretase activities associated with lipid rafts isolated from AD, MCI and control cortices (Brodmann areas 9–11). For definite confirmation of the Aβ species, the reaction mixtures were subjected to quantitative Western blotting using specific antibodies rather than ELISA. At time 0, deposited Aβ42/43 species were detected in rafts from MCI/AD brains but not in control specimen (Supporting Information Fig S3). The amounts of ln(Aβ38 + Aβ42), which reflect the total capacity of the Aβ38/42-producing line, did not vary between AD, MCI and controls (Supporting Information Fig S4; $p = 0.969$, ANOVA). Thus, the gross activities of raft γ-secretase were comparable among the three groups. However, the plotted values for Aβ40/43 *versus* Aβ38/42 are divided into two groups: MCI/AD and controls (Fig 5; Aβ40/43 for control *vs.* MCI/AD, $p < 0.001$; Aβ38/42 for control *vs.* MCI/AD, $p = 0.001$; Welch's *t*-test) in the same way as those derived from CSF (Fig 4). It is notable that Figs. 4 and 5 are based on different methods, ELISA and Western blotting, respectively, but give similar results. There were no significant differences between MCI and AD specimen, although MCI patients (91 ± 4.9-year-old) were older than controls (77 ± 6.5-year-old) or AD patients (80 ± 5.0-year-old) (Aβ40/43 for MCI *vs.* AD, $p = 0.342$; Aβ38/42 for MCI *vs.* AD, $p = 0.911$). There were similar significant differences between control *versus* AD in the groups of which the ages were not significantly different (Aβ40/43 for control *vs.* AD, $p < 0.001$; Aβ38/42 for control *vs.* AD, $p = 0.03$).

DISCUSSION

Here, we assume that (i) Aβs in CSF are produced exclusively by γ-secretase in the brain, possibly in neurons; and (ii) Aβs in CSF are in the steady state. With these assumptions, the combined measurement of four Aβ species in CSF should predict the activity of γ-secretase in the brain. Here, the alterations in the γ-secretase activities do not mean the gross activity, *i.e.* total Aβ production, but the cleavage efficiency of the intermediates, Aβ42 and Aβ43.

In the present study, we quantified in CSF the four Aβ species, Aβ38/42 and Aβ40/43, but the Western blotting indicated the presence of additional Aβ species, Aβ37 and 39, in CSF (Supporting Information Fig S2). At present, we cannot exclude the possibility that a certain carboxyl terminus-specific protease(s) in CSF acts on the pre-existing Aβ species and converts them to Aβ37 and 39 (Zou et al, 2007). However, according to our unpublished data (Takami et al, unpublished observations), it is plausible that Aβ37 is derived from Aβ40, whereas Aβ39 is derived from Aβ42. Even if so, these pathways are very minor (~20–100-fold less) compared to the two major pathways, Aβ42 to Aβ38, and Aβ43 to Aβ40, when assessed by a reconstituted system (Takami et al, 2009). Thus, such strict relationships between four Aβs may have been relatively independent of Aβ37 and 39. The detailed relationship between all Aβs in the CSF awaits further quantification of the additional two Aβ species.

Currently, we do not know why the observation that Aβ40 is higher in MCI/AD CSF has so far not been reported except a recent paper (Simonsen et al, 2007). In fact, some of us previously reported no significant differences in CSF Aβ40 between AD and control subjects using a different ELISA (Shoji et al, 1998). It may be notable that we used newly constructed ELISA for Aβ40 based on a different set of monoclonal antibodies and thus, those discrepancies may come from the different antibody/epitope combination used for ELISA and/or different assay methods. In particular, it should be noted that all ELISAs used here detect Aβ1-x only, but not amino-terminally truncated forms. In this context, the ratio of Aβ40/43 appears to be more informative to discriminate between control and MCI/AD than the absolute levels of Aβ40 alone (Table 1 and Fig 5). It is possible that even if Aβ40 is not different between control and MCI/AD, the ratio Aβ40/43 could discriminate them.

We are the first to measure CSF Aβ43 using ELISA. The CSF concentrations of Aβ43 are 10-fold less than those of Aβ42. Nevertheless, the specificity of the newly constructed ELISA made the quantification of accurate levels of Aβ43 possible (Supporting Information Fig S1). Regarding the Aβ43 measures, we observed that its behaviour is entirely similar to that of Aβ42 in MCI/AD. Our preliminary observations using immunocytochemistry and ELISA quantification strongly suggest that Aβ43 deposits in aged human brains at the same time as Aβ42 (unpublished observations). Furthermore, Saido and colleagues have only recently reported that a PS1 R278I mutation in mice (heterozygous) caused an elevation of Aβ43 and its early and pronounced accumulation in the brain (Saito et al, 2011). It is possible that the cleavage of βCTF by this R278I γ-secretase may

be profoundly suppressed in the third cleavage step of the product line 1 (see Fig 1), which would result in negligible levels of Aβ40 and unusually high levels of Aβ43 (Nakaya et al, 2005). These results suggest that the role of Aβ43 should be reconsidered for the initiation of β-amyloid deposition and thus in AD pathogenesis.

Lower CSF concentrations of Aβ42 and 43 are not exclusively limited to MCI/AD. For example, similar low concentrations of Aβ42 and 43 were found in the CSF from eight patients with idiopathic normal pressure hydrocephalus (iNPH) (Aβ42, 76.3 ± 37.3 pM, $p = 0.012$ compared to controls: Aβ43, 5.2 ± 2.9 pM, $n = 8$, $p = 0.004$ compared to controls: Bonferroni's *t*-test; Silverberg et al, 2003). Thus, lower CSF concentrations of Aβ42 and 43 alone were unable to distinguish between iNPH and MCI/AD, and further, it is claimed that the former is often associated with abundant senile plaques, raising the possibility that Aβ deposition is enhanced by iNPH (Silverberg et al, 2003). However, when their partners Aβ38 and 40 were measured in CSF, both were found not to be significantly increased in iNPH (Aβ38, 459.2 ± 138.5 pM, $p = 0.484$ compared to controls; Aβ40, 1094.4 ± 375.3 pM, $n = 8$, $p = 0.103$ compared to controls; Table 1) in sharp contrast to MCI/AD indicating that the cleavage in iNPH at the steps from Aβ43 to 40 and from Aβ42 to 38 is not enhanced as it is in MCI/AD. Thus, it may be that the dilution effect elicited by ventricular enlargement would be the cause of lower CSF Aβ42 and 43 found in iNPH.

Currently, we do not know the mechanism behind the altered activity of brain γ-secretase in MCI/AD (Fig 4). First, it is of note that rafts prepared from MCI/AD brains but never from control brains at SP stage 0/A accumulated Aβ42 and Aβ43 (Supporting Information Fig S3; Oshima et al, 2001). It is possible that raft-deposited Aβ42/43 could induce a change in the γ-secretase activity, although the extent of the alteration in the activity appears not to be related to the extent of accumulation (unpublished observation). In this regard, it is of interest to note that Tg2576 mice, the best characterized AD animal model, shows reduced levels of Aβ42 in plasma as well as in CSF at the initial stage of Aβ deposition (Kawarabayashi et al, 2001). If the assumption here is correct, this may suggest that γ-secretase that produces plasma Aβs could also be altered. However, thus far, we have failed to replicate significantly lower Aβ42 levels or Aβ42/Aβ40 ratios in plasma from AD patients.

Second, there could be heterogenous populations of γ-secretase complexes that have distinct activities due to subtle differences in their components. γ-Secretase is a complex of four membrane proteins including PS, nicastrin (NCT), anterior pharynx defective 1 (Aph1) and presenilin enhancer 2 (Pen 2) (Takasugi et al, 2003). Aph 1 has three isoforms, and each can assemble active γ-secretase together with other components (Serneels et al, 2009). NCT, a glycoprotein, is present in immature and mature forms (Yang et al, 2002). The abundance of these heterogenous populations of proteins in the brain is probably under strict control. During MCI/AD, a certain population could replace other populations of γ-secretase and thus may show a distinct activity as a whole.

The data shown here represent only a cross-sectional study, but our keen interest is how the CSF levels of the four Aβ species would shift during the longitudinal course in an individual who is going to develop sporadic AD. Does one have any period during life when Aβ42 and 43 are at higher levels in CSF, and thus the ratios of Aβ38/42 and Aβ40/43 are smaller? At this period when the final cleavage steps of γ-secretase would be suppressed, the ISF concentrations of Aβ43 and 42 would increase, which would start or promote their aggregation in the brain parenchyma. If so, during life span, the individual's plot would move down along the regression line and move up as senile plaques accumulate, and the individual would eventually develop sporadic AD. However, thus far the period when there are increases in CSF Aβ42/43 has never been reported for sporadic AD. Nor has it been reported for asymptomatic FAD carriers (Ringman et al, 2008), whereas their plasma is known to contain higher levels (and percent) of Aβ42 (Kosaka et al, 1997; Ringman et al, 2008; Scheuner et al, 1996). It is likely that the stage of normal cognition and Aβ accumulation already accompanies reduced CSF Aβ42. If so, the alterations of γ-secretase should continue on for decades. Most interestingly, this alteration of CSF Aβ regulation seems to be planned to prevent further accumulation of Aβ42 and 43 in the brain.

However, Hong et al (2011) have recently shown, using *in vivo* microdialysis to measure ISF Aβ in APP transgenic mice, that the increasing parenchymal Aβ is closely correlated with decreasing ISF Aβ, suggesting that produced Aβ42 is preferentially incorporated into existing plaque-Aβ. This is a prevailing way of the interpretation of the data. Another way of the interpretation of data would be that during aging from 3 to 24 months, γ-secretase activity becomes altered and produces decreasing amounts of Aβ but with an increasing ratio of Aβ38/42 (and Aβ40/43). It is worth to mention that produced Aβ42 (but not Aβ40) appears to be selectively bound to rafts (from CHO cells) after long incubation (>4 h; Wada et al, unpublished observation). Also of note is that we quantified the total (free and bound) Aβ produced by an *in vitro* reconstituted system (Fig 5). What is claimed here is that decreased levels of CSF Aβ42 are largely due to alterations of γ-secretase activity rather than due to selective deposition of Aβ42 in preexisting plaques. What proportions of decreased ISF (CSF) Aβ42 levels would be contributed to by altered γ-secretase activity and selective deposition of Aβ42/43 to parenchymal plaques awaits future studies.

Finally, our observation has therapeutic implication. As shown elsewhere and here above, if Aβ42 is the culprit for MCI/AD, non-steroidal anti-inflammatory drugs (NSAIDs) would have been quite a reasonable therapeutic compound, which enhances cleavage at the third step in the stepwise processing, leading to lower levels of Aβ42 without greatly interfering with the Aβ bulk flow (Weggen et al, 2001). This sharply contrasts with some of the γ-secretase inhibitors currently under development and in clinical trial, which block the Aβ bulk flow. However, the present study raises the possibility that even if NSAIDs are administered, the expected beneficial effect could be minimal in MCI/AD patients, because in these patient brains, γ-secretase is already shifted to an NSAID-like effect.

MATERIALS AND METHODS

Subjects

Cerebrospinal fluid samples from 24 AD patients (mild to moderate AD; 50–86 years old), 19 MCI patients (57–82 years old) and 21 control subjects (61–89 years old) were collected (see Table 1) at Department of Neurology, Hirosaki University Hospital and at Department of Geriatrics and Gerontology, Tohoku University Hospital, and at Department of Neurology, Niigata University Hospital. The CSF samples from (symptomatic) 5 FAD (mPS1) patients (T116N, L173F, G209R, L286V and L381V) were from Niigata University Hospital. Probable AD cases met the criteria of the National Institute of Neurological and Communicative Disorders and Stroke–Alzheimer's Disease and Related Disorders (NINCDS-ADRDA) (Kuwano et al, 2006; McKhann et al, 1984). Additional diagnostic procedures included magnetic resonance imaging. Dementia severity was evaluated by the Mini-Mental State Examination (MMSE). Diagnosis of MCI was made according to the published criteria (Winblad et al, 2004). Diagnosis of iNPH was made according to the guideline issued by the Japanese Society of NPH (Ishikawa et al, 2008). Controls who had no sign of dementia and lived in an unassisted manner in the local community were recruited. All individuals included in this study were Japanese and 24 AD patients examined here were judged to have sporadic AD because of negative family history. This study was approved by the ethics committee at each hospital or institute.

Human cortical specimens for quantification of raft-associated γ-secretase activity were obtained from those brains that were removed, processed and placed in −80°C within 12 h postmortem [Patients were placed in a cold (4°C) room within 2 h after death] at the Brain Bank at Tokyo Metropolitan Institute of Gerontology. For all the brains registered at the bank we obtained written informed consents for their use for medical research from patient or patient's family. Each brain specimen (~0.5 g) were taken from Brodmann areas 9–11 of 13 AD patients [80 ± 5.0 years of age, Braak NFT stage > IV, SP stage = C (retrospective) CDR ≫ 1], 10 MCI patients (91 ± 4.9 years of age, Braak NFT stage < IV, SP stage < C, CDR = 0.5) and 16 controls (77 ± 6.5 years of age, Braak NFT stage < I, SP stage = 0/A, CDR = 0) (Adachi et al, 2010; Li et al, 1997).

Cerebrospinal fluid analysis

Cerebrospinal fluid (10–15 ml) was collected in a polypropylene or polystyrene tube and gently inverted. After brief centrifugation CSF was aliquotized to polypropylene tubes (0.25–0.5 ml), which were kept at −80°C until use. In our experience, Aβ42 (possibly, other Aβ species too) are readily absorbed even to polypropylene tubes (~20% per new exposure, as shown by Luminex xMAP quantification), and repeated aliquotization to new tubes may cause profoundly lower measures of Aβs (Tsukie and Kuwano, unpublished data, 2010). This may partly explain why absolute levels of Aβs in CSF greatly vary among laboratories, whereas their relative ratios (*e.g.* Aβ42/40) seem to be roughly consistent. The CSF concentrations of Aβ38, 40 and 42 were quantified using commercially available ELISA kits (Cat no. 27717, 27718 and 27712, respectively, IBL, Gunma, Japan). To measure Aβ43, anti-Aβ43 polyclonal antibody as a capture antibody was combined with amino terminus-specific antibody (82E1) (Cat no. 10323, IBL, Gunma, Japan) as a detector antibody. The detection limit of Aβ43 quantified by the ELISA was 0.78 pM (data not shown). Thus all ELISAs used here detect Aβ1-x, but not amino-terminally truncated Aβs. The specificities of ELISAs are provided in Supporting Information Fig S1.

CSF immunoprecipitation and Western blotting

When required, CSF Aβs were immunoprecipitated with protein G-sepharose conjugated with 82E1 at 4°C by keeping a container in gentle rotation overnight. The mixture was centrifuged at 10,000×g for 5 min, and resultant pellets were then washed twice with phosphate-buffered saline. The washed beads were suspended with the Laemmli sample buffer for SDS–polyacrylamide gel electrophoresis (SDS–PAGE). The immunoprecipitated Aβs were separated on Tris/Tricine/8 M urea gels (Kakuda et al, 2006), followed by Western blotting using 82E1. To immunodetect Aβ42 and Aβ43, Aβ42 monoclonal antibody (44A3, IBL) and Aβ43 polyclonal antibody (IBL) were used (Supporting Information Fig S3).

Numerical simulation based on the stepwise processing model of γ-secretase

The temporal profiles for the ratios of Aβ40/43 and Aβ38/42 were simulated based on the stepwise processing model. Parameters including rate constants were set to fit maximally the temporal profile of the cleaving activity in the reconstituted γ-secretase system (Takami et al, 2009).

We set the condition that βCTF substrate is supplied steadily from the external source. When βCTF supply is balanced roughly in the order with γ-secretase processing rate, the stepwise-processing model was found to have the two successive steady states, with each accompanying linear changes in [ES] or [S] concentrations. The first steady state is just after the initial transition period that corresponds to the acute saturation phase of γ-secretase with βCTF. The second steady state is associated with the constant concentrations of the enzyme/substrate complex except ES38 and ES40. Because these steady states kept the ratios of Aβ38/Aβ40 and Aβ42/Aβ43 constant, the simulation was quite consistent with the CSF data.

Quantification of human brain raft-associated γ-secretase activity

Since γ-secretase is thought to be concentrated in rafts (Hur et al, 2008; Wada et al, 2003), we measured raft-associated γ-secretase activity rather than CHAPSO-solubilized activity. Rafts were prepared from human brains which were frozen within 12 h postmortem, as previously described (Oshima et al, 2001; Wada et al, 2003) with some modifications. We do not know exactly whether the γ-secretase activity depends upon the sampling site. In our hands, there appear no large differences in the activity among the sampled sites in a given prefrontal slice. No significant differences in the activity were noted between outer and inner layer of the cortex. After carefully removing leptomeninges and blood vessels, small (<0.5 g) blocks from prefrontal cortices (Brodmann areas 9–11) were homogenized in ~10 volumes of 10% sucrose in MES-buffered saline (25 mM MES, pH 6.5, and 150 mM NaCl) containing 1% CHAPSO and various protease inhibitors. The homogenate was adjusted to 40% sucrose by the addition of an equal volume of 70% sucrose in MES-buffered saline, placed at the bottom of an ultracentrifuge tube, and overlaid with 4 ml of 35% sucrose and finally with 4 ml of 5% sucrose in MES-buffered saline. The discontinuous gradient was centrifuged at 39,000 rpm for 20 h at 4°C on a SW 41 Ti rotor (Beckman, Palo

The paper explained

PROBLEM:

Alzheimer's disease is a devastating form of progressive dementia, in which senile plaques composed of Aβ form in the brain. Different species of Aβ are derived from APP through sequential cleavage by β- and γ-secretases and can be detected in the CSF of patients. These can serve as markers for the disease.

RESULTS:

We investigated why CSF concentrations of Aβ42 are lower in MCI and AD patients. We suggest that this is not because Aβ42/43 is selectively deposited in the brain, but because γ-secretase activity is altered in AD brain: more Aβ42 and Aβ43 are converted to Aβ40 and Aβ38, respectively, resulting in lower Aβ42 and Aβ43 in CSF.

IMPACT:

Our results predict that γ-secretase modulators would have only limited efficacy in treatment of AD patients, because Aβ42/43 production by γ-secretase is already shifted towards reduced levels in AD brain.

Alto, CA). An interface of 5%/35% sucrose (fraction 2) was carefully collected (referred to as raft fraction). Raft fractions were recentrifuged after dilution with buffer C (20 mM PIPES, pH 7.0, 250 mM sucrose and 1 mM EGTA). The resultant pellet was washed twice and resuspended with buffer C, which was kept at −80°C until use.

As the method of measuring the raft γ-secretase activity was not yet established, we first determined the assay conditions. The incubation of raft fraction with βCTF generated exactly the same tri- and tetrapeptides we previously observed in the detergent-soluble γ-secretase assay system (Takami et al, unpublished observation). This suggests that the cleavage by raft-associated γ-secretase proceeds in the identical manner as by CHAPSO-reconstituted γ-secretase (Takami et al, 2009). In our hands, preexisting βCTF bound in rafts generated only negligible amounts of Aβs, and their generation was dependent exclusively on exogenously added βCTF. Thus, we concluded that the addition of βCTF to raft fraction make possible to measure the raft-associated γ-secretase activity, although we do not know how the exogenously added βCTF is integrated into raft, gets access to and is degraded by raft-embedded γ-secretase. Using this assay method, the activities of raft-associated γ-secretase in human brains were found to be only a little affected postmortem, when compared with that prepared from fresh rat brains. A progressive decline in the activity was barely detectable from 4 to 17 h postmortem. The discrepancy in the postmortem decay between our and the previous data (Hur et al, 2008) would be ascribed to the assay method: the latter are based on the activity measured by using endogenous (raft-bound) substrate that is also susceptible to proteolytic degradation (Hur et al, 2008).

Each raft fraction, adjusted to 100 μg/ml in protein concentration, was incubated with 200 nM C99FLAG for 2 h at 37°C (Kakuda et al, 2006). The produced Aβs were separated on SDS–PAGE, and subjected to quantitative Western blotting, using specific antibodies, 3B1 for Aβ38, BA27 for Aβ40, 44A3 for Aβ42 and anti-Aβ43 polyclonal for Aβ43.

Statistical analysis

All statistical analyses were performed using SPSS version 14.0. The results were expressed as means ± standard deviations. Because data transformations were required to achieve normally distributed data, all analyses including Aβ38, Aβ40, Aβ42 and Aβ43 were performed after a logarithmic transformation. Pearson's correlation coefficients were calculated to indicate the strength of the linear relationship between two variables. An ANOVA was used to test the equality of mean values of continuous variables among three groups, that is control, MCI and AD. Multiple comparisons were done by Dunnett's *t*-test, Bonferroni's *t*-test and Welch's *t*-test between control and MCI/AD, and among three groups, respectively. A two-tailed *p*-value of <0.05 was considered to be statistically significant.

Author contributions

NK, MT, KN, YI: measurement of raft-associated γ-secretase activity in human brains, LC-MS/MS confirmation of released peptides, ELISA quantification of Aβ38, 40, 42 and 43 in CSF and tissue blocks, and experimental design of the present work; MS, HiA, KF, TI, and the Japanese Alzheimer's Disease Neuroimaging Initiative: collection of CSF samples from controls, MCI/AD patients; YH, MM, HaA: collection of CSF from iNPH patients; HY, SM, HH: Aβ immunocytochemistry of tissue sections from brains with various SP stages (Braak); KA: statistical analysis; RK: establishment of the appropriate Aβ quantification conditions; YN: simulation of the stepwise processing model.

Acknowledgements

We thank Dr. Haruhiko Akiyama, Department of Psychogeriatrics, Tokyo Institute of Psychiatry, Tokyo Metropolitan Organization for Medical Research, Tokyo, for the help in the initial phase of this study, and Dr. Takaomi C. Saido, RIKEN Brain Science Institute, for sharing the data on his R278I transgenic mice. Dr. Makoto Higuchi, Molecular Imaging Center, National Institute of Radiological Sciences, Chiba, kindly provided us with aged Tg2576 littermates. This project was supported by New Energy and Industrial Technology Development Organization in Japan (J-ADNI).

Supporting Information is available at EMBO Molecular Medicine online.

The authors declare that they have no conflict of interest.

References

Adachi T, Saito Y, Hatsuta H, Funabe S, Tokumaru AM, Ishii K, Arai T, Sawabe M, Kanemaru K, Miyashita A, *et al* (2010) Neuropathological asymmetry in argyrophilic grain disease. J Neuropathol Exp Neurol 69: 737-744

Hong S, Quintero-Monzon O, Ostaszewski BL, Podlisny DR, Cavanaugh WT, Yang T, Holtzman DM, Cirrito JR, Selkoe DJ (2011) Dynamic analysis of amyloid β-protein in behaving mice reveals opposing changes in ISF versus parenchymal Aβ during age-related plaque formation. J Neurosci 31: 15861-15869

Hur JY, Welander H, Behbahani H, Aoki M, Frånberg J, Winblad B, Frykman S, Tjernberg LO (2008) Active gamma-secretase is localized to detergent-resistant membranes in human brain. FEBS J 275: 1174-1187

Ishikawa M, Hashimoto M, Kuwana N, Mori E, Miyake H, Wachi A, Takeuchi T, Kazui H, Koyama H (2008) Guidelines for management of idiopathic normal pressure hydrocephalus. Neurol Med Chir (Tokyo) 48: S1-S23

Iwatsubo T, Odaka A, Suzuki N, Mizusawa H, Nukina N, Ihara Y (1994) Visualization of Aβ42(43) and Aβ40 in senile plaque with end-specific Aβ monoclonals: evidence that an initially deposited forms is Aβ42(43). Neuron 13: 45-53

Kakuda N, Funamoto S, Yagishita S, Takami M, Osawa S, Dohmae N, Ihara Y (2006) Equimolar production of amyloid β-protein and amyloid precursor protein intracellular domain from β-carboxyl-terminal fragment by γ-secretase. J Biol Chem 281: 14776-14786

Kawarabayashi T, Younkin LH, Saido TC, Shoji M, Ashe KH, Younkin SG (2001) Age-dependent changes in brain, CSF, and plasma amyloid (β) protein in the Tg2576 transgenic mouse model of Alzheimer's disease. J Neurosci 21: 372-381

Kosaka T, Imagawa M, Seki K, Arai H, Sasaki H, Tsuji S, Asami-Odaka A, Fukushima T, Imai K, Iwatsubo T (1997) The βAPP717 Alzheimer mutation increases the percentage of plasma amyloid-beta protein ending at Aβ42(43). Neurology 48: 741-745

Kuwano R, Miyashita A, Arai H, Asada T, Imagawa M, Shoji M, Higuchi S, Urakami K, Kakita A, Takahashi H, *et al* (2006) Dynamin-binding protein gene on chromosome 10q is associated with late-onset Alzheimer's disease. Hum Mol Genet 15: 2170-2182

Li G, Aryan M, Silverman JM, Haroutunian V, Perl DP, Birstein S, Lantz M, Marin DB, Mohs RC, Davis KL (1997) The validity of the family history method for identifying Alzheimer disease. Arch Neurol 54: 634-640

McKhann G, Drachman D, Folstein M, Katzman R, Price D, Stadlan EM (1984) Clinical diagnosis of Alzheimer's disease: report of the NINCDS-ADRDA Work Group under the auspices of Department of Health and Human Services Task Force on Alzheimer's Disease. Neurology 34: 939-944

Nakaya Y, Yamane T, Shiraishi H, Wang HQ, Matsubara E, Sato T, Dolios G, Wang R, De Strooper B, Shoji M, *et al* (2005) Random mutagenesis of presenilin-1 identifies novel mutants exclusively generating long amyloid β-peptides. J Biol Chem 280: 19070-19077

Oshima N, Morishima-Kawashima M, Yamaguchi H, Yoshimura M, Sugihara S, Khan K, Games D, Schenk D, Ihara Y (2001) Accumulation of amyloid beta-protein in the low-density membrane domain accurately reflects the extent of beta-amyloid deposition in the brain. Am J Pathol 158: 2209-2218

Qi-Takahara Y, Morishima-Kawashima M, Tanimura Y, Dolios G, Hirotani N, Horikoshi Y, Kametani F, Maeda M, Saiso TC, Wang R, *et al* (2005) Longer forms of amyloid β protein: implications for the mechanism of intramembrane cleavage by γ-secretase. J Neurosci 25: 436-445

Ringman JM, Younkin SG, Pratico D, Seltzer W, Cole GM, Geschwind DH, Rodriguez-Agudelo Y, Schaffer B, Fein J, Sokolow S, *et al* (2008) Biochemical markers in persons with preclinical familial Alzheimer disease. Neurology 71: 85-92

Saito T, Suemoto T, Brouwers N, Sleegers K, Funamoto S, Mihira N, Matsuba Y, Yamada K, Nilsson P, Takano J, *et al* (2011) Potent amyloidogenicity and pathogenicity of Aβ43. Nat Neurosci 14: 1023-1032

Scheuner D, Eckman C, Jensen M, Song X, Citron M, Suzuki N, Bird TD, Hardy J, Hutton M, Kukull W, *et al* (1996) Secreted amyloid β-protein similar to that in the senile plaques of Alzheimer's disease in increase in vivo by the presenilin 1 and 2 and APP mutations linked to familial Alzheimer's disease. Nat Med 2: 864-870

Schoonenboom NS, Mulder C, Van Kamp GJ, Mehta SP, Scheltens P, Blankenstein MA, Mehta PD (2005) Amyloid β 38, 40, and 42 species in cerebrospinal fluid: more of the same. Ann Neurol 58: 139-142

Selkoe DJ (2001) Alzheimer's disease: genes, proteins, and therapy. Physiol Rev 81: 741-766

Serneels L, Van Biervliet J, Craessaerts K, Dejaegere T, Horre K, Van Houtvin T, Esselmann H, Paul S, Schafer MK, Berezovska O, *et al* (2009) γ-Secretase heterogeneity in the Aph1 subunit: relevance for Alzheimer's disease. Science 324: 639-642

Shoji M, Matsubara E, Kanai M, Watanabe M, Nakamura T, Tomidokoro Y, Shizuka M, Wakabayashi K, Igeta Y, Ikeda Y, *et al* (1998) Combination assay of CSF tau, Aβ1–40 and Aβ 1–42(43) as a biochemical marker of Alzheimer's disease. J Neurol Sci 158: 134-140

Silverberg GD, Mayo M, Saul T, Rubenstein E, McGuire D (2003) Alzheimer's disease, normal-pressure hydrocephalus, and senescent changes in CSF circulatory physiology: a hypothesis. Lancet Neurol 2: 506-511

Simonsen AH, Hansson SF, Ruetschi U, McGuire J, Podust VN, Davies HA, Mehta P, Waldemar G, Zetterberg H, Andreasen N, *et al* (2007) Amyloid β1–40 quantification in CSF: comparison between chromatographic and immunochemical methods. Dement Geriatr Cogn Disord 23: 246-250

Takami M, Nagashima Y, Sano Y, Ishihara S, Morishima-Kawashima M, Funamoto S, Ihara Y (2009) γ-Secretase: successive tripeptide and tetrapeptide release from the transmembrane domain of β-carboxyl terminal fragment. J Neurosci 29: 13042-13052

Takasugi N, Tomita T, Hayashi I, Tsuruoka M, Niimura M, Takahashi Y, Thinakaran G, Iwatsubo T (2003) The role of presenilin cofactors in the γ-secretase complex. Nature 422: 438-441

Wada S, Morishima-Kawashima M, Qi Y, Misonou H, Shimada Y, Ohno-Iwashita Y, Ihara Y (2003) Gamma-secretase activity is present in rafts but is not cholesterol-dependent. Biochemistry 47: 13977-13986

Weggen S, Eriksen JL, Das P, Sagi SA, Wang R, Pietrzik CU, Findlay KA, Smith TE, Murphy MP, Bulter T, *et al* (2001) A subset of NSAIDs lower amyloidogenic Aβ42 independently of cyclooxygenase activity. Nature 414: 212-216

Winblad B, Palmer K, Kivipelto M, Jelic V, Fratiglioni L, Wahlund LO, Nordberg A, Backman L, Albert M, Almkvist O, *et al* (2004) Mild cognitive impairment—beyond controversies, towards a consensus: report of the International Working Group on Mild Cognitive Impairment. J Intern Med 256: 240-246

Yang DS, Tandon A, Chen F, Yu G, Yu H, Arakawa S, Hasegawa H, Duthie M, Schmidt SD, Ramabhadran TV, *et al* (2002) Mature glycosylation and trafficking of nicastrin modulate its binding to presenilins. J Biol Chem 277: 28135-28142

Zou K, Yamaguchi H, Akatsu H, Sakamoto T, Ko M, Mizoguchi K, Gong JS, Yu W, Yamamoto T, Kosaka K, *et al* (2007) Angiotensin-converting enzyme converts amyloid β-protein 1–42 (Aβ(1–42)) to Aβ(1–40), and its inhibition enhances brain Aβ deposition. J Neurosci 27: 8628-8635

